bioRxiv preprint doi: https://doi.org/10.1101/2022.09.29.510137; this version posted September 30, 2022. The copyright holder for this preprint (which was not certified by peer review) is the author/funder, who has granted bioRxiv a license to display the preprint in perpetuity. It is made available under aCC-BY-NC-ND 4.0 International license.

LKB1 loss rewires JNK-induced apoptotic protein dynamics through NUAKs and sensitizes *KRAS*-mutant NSCLC to combined KRAS^{G12C} + MCL-1 blockade

Chendi Li[1, 2], Mohammed Usman Syed[1], Yi Shen[1], Cameron Fraser[3], Jian Ouyang[1], Johannes Kreuzer[1], Sarah E. Clark[1], Audris Oh[1], Makeba Walcott[1], Robert Morris[1], Christopher Nabel[1,5], Sean Caenepeel[4], Anne Y. Saiki[4], Karen Rex[4], J. Russell Lipford[4], Rebecca S. Heist[1,2], Jessica J. Lin[1,2], Wilhelm Haas[1], Kristopher Sarosiek[3], Paul E. Hughes[4], Aaron N. Hata[1,2].

Affiliations:

[1]Massachusetts General Hospital Cancer Center, Charlestown, Massachusetts.

[2]Department of Medicine, Massachusetts General Hospital and Harvard Medical School, Boston, Massachusetts.

[3]Harvard T.H. Chan School of Public Health, Laboratory of Systems Pharmacology (Harvard Medical School), Boston, Massachusetts

[4]Amgen Research, Amgen Inc., Thousand Oaks, California

[5]Massachusetts Institute of Technology, Cambridge, Massachusetts.

Corresponding Author:

Aaron N. Hata, MD, PhD, Massachusetts General Hospital Cancer Center, 149 13th Street, Charlestown, MA 02129. Phone: 617-724-3442; E-mail: ahata@mgh.harvard.edu

Running Title: *KRAS*-mutant LKB1-deficient NSCLCs are sensitive to combined KRAS^{G12C} + MCL-1 inhibition

Keywords: KRAS, *STK11*/LKB1, MCL-1, non-small cell lung cancer, apoptosis

Figures: 7 main, 9 supplemental

bioRxiv preprint doi: https://doi.org/10.1101/2022.09.29.510137; this version posted September 30, 2022. The copyright holder for this preprint (which was not certified by peer review) is the author/funder, who has granted bioRxiv a license to display the preprint in perpetuity. It is made available under aCC-BY-NC-ND 4.0 International license.

ABSTRACT

The recently approved KRAS^{G12C} inhibitor sotorasib induces durable responses of *KRAS*^{G12C}-mutant non-small cell lung cancers (NSCLCs), however, some patients do not derive benefit. Identification of specific vulnerabilities conferred by co-occurring mutations may enable the development of biomarker-driven combination therapies in distinct subsets of patients. We report that co-occurring loss of *STK11*/LKB1 is associated with a drug-induced vulnerability of *KRAS*-mutant NSCLCs to MCL-1 inhibition. In LKB1-deficient cells, inhibition of KRAS-MAPK signaling leads to hyperactivated JNK, which phosphorylates BCL-XL and impairs its ability to sequester BIM, thus creating a dependency on MCL-1 for survival. In LKB1-proficient cells, LKB1 suppresses drug-induced JNK hyperactivation in a NUAK-dependent manner. *Ex vivo* treatment of tumors from LKB1-deficient but not LKB1 wild-type *KRAS*-mutant NSCLC patients with sotorasib or trametinib increased MCL-1 dependence. These results uncover a novel role for the LKB1-NUAK axis in regulation of apoptotic dependency and suggest a genotype-directed therapeutic approach for KRAS-LKB1 mutant NSCLC.

bioRxiv preprint doi: https://doi.org/10.1101/2022.09.29.510137; this version posted September 30, 2022. The copyright holder for this preprint (which was not certified by peer review) is the author/funder, who has granted bioRxiv a license to display the preprint in perpetuity. It is made available under aCC-BY-NC-ND 4.0 International license.

INTRODUCTION

Mutations in KRAS, a small GTPase that regulates MAPK/ERK signaling, define the largest genetically-defined subset of non-small cell lung cancer, representing 25-30% of all lung adenocarcinomas (Cancer Genome Atlas Research, 2014). The recent approval of sotorasib (AMG 510) (Canon et al., 2019), a small molecule covalent $KRAS^{G12C}$-selective inhibitor, marked a milestone in the development of targeted therapies for KRAS-mutant cancers. While most NSCLC patients treated with sotorasib experience clinical benefit, only ~40% achieve a partial response (Skoulidis et al., 2021). Similar results have been reported for other $KRAS^{G12C}$ inhibitors in development (Janne et al., 2022) that similarly target the inactive GDP-bound form of KRAS. Preclinical studies have suggested that efficacy may be limited by upstream receptor tyrosine kinase (RTK) activity (which can drive KRAS into the GTP-bound form)(Xue et al., 2020), concurrent activation of parallel signaling pathways (Misale et al., 2019) (Lou et al., 2019) and feedback reactivation of MAPK signaling (Ryan et al., 2020). Drug combination strategies designed to target these mechanisms (e.g., with EGFR, SHP2 or MEK inhibitors), as well as other empiric combinations (e.g., with chemotherapy or immune checkpoint inhibitors) are currently being tested in the clinic.

KRAS-mutant lung cancers harbor diverse co-occurring mutations (Cancer Genome Atlas Research, 2014), and although not yet fully characterized, emerging evidence indicates that some mutations may predict lack of response to different therapies. For instance, co-occurring *STK11* or *KEAP1* mutations predict poor response of *KRAS*-mutant lung cancers to anti-PD-(L)1 immune checkpoint inhibitors (Skoulidis et al., 2018), and co-occurring *KEAP1* mutations may additionally be associated with decreased sensitivity to $KRAS^{G12C}$ inhibitors (Skoulidis *et al.*, 2021) (Janne *et al.*, 2022). Co-occurring mutations that positively predict response to $KRAS^{G12C}$ inhibitors or drug combinations have yet to be reported. Considering the genetic heterogeneity of *KRAS*-mutant lung cancers, and the multitude of drug combinations entering clinical testing, it is crucial to identify vulnerabilities conferred by specific genomic alterations and develop biomarkers that can predict response to $KRAS^{G12C}$ inhibitor combinations and help guide patient selection.

Preclinical studies have demonstrated that knockdown or suppression of KRAS or downstream signaling in *KRAS*-mutant cell lines often fails to induce apoptosis (Singh et al., 2009) (Corcoran et al., 2013) (Hata et al., 2014). Suppression of MEK/ERK signaling leads to the accumulation of the pro-apoptotic BCL-2 family protein BIM, which is critical for inducing apoptosis in response to an array of targeted therapies (Cragg et al., 2008) (Hata et al., 2015). However, induction of BIM by MEK or $KRAS^{G12C}$ inhibition alone is often insufficient to induce apoptosis in *KRAS*-mutant cancer cells because BIM is bound and neutralized by pro-survival BCL-2 family proteins such as BCLX-XL or MCL-1. Combining MEK inhibitors with BH3 mimetics, which competitively bind to BCL-XL or MCL-1 and liberate BIM, can induce apoptosis and lead to regression of *KRAS*-mutant tumors (Corcoran *et al.*, 2013) (Nangia et al., 2018) (Cragg et al., 2009). However, clinically relevant biomarkers that can differentiate specific apoptotic dependencies (MCL-1 versus BCL-XL) and thus stratify patients for treatment with $KRAS^{G12C}$ inhibitor + BH3 mimetic combinations are lacking.

While studying the response of *KRAS*-mutant lung cancer models to $KRAS^{G12C}$ or MEK inhibitors combined with BH3 mimetics, we unexpectedly observed an association between the presence of *STK11* mutations and dependence on MCL-1. *STK11*, which encodes the protein LKB1 (Liver Kinase B1), is inactivated in approximately 30% of *KRAS*-mutant lung cancers (Kandoth et al., 2013). Given that LKB1 loss has been associated with poor prognosis (Ji et al., 2007) (Chen et al., 2012) (Wingo et al., 2009) and diminished response to immune checkpoint inhibitors (Skoulidis *et al.*, 2018), there is a critical need to develop new therapeutic approaches for these

bioRxiv preprint doi: https://doi.org/10.1101/2022.09.29.510137; this version posted September 30, 2022. The copyright holder for this preprint (which was not certified by peer review) is the author/funder, who has granted bioRxiv a license to display the preprint in perpetuity. It is made available under aCC-BY-NC-ND 4.0 International license.

patients. Here, we describe a novel mechanism by which LKB1 suppresses JNK stress signaling via its substrate effectors NUAK1/2. Upon treatment with sotorasib or trametinib (MEK inhibitor), LKB1-deficient cells hyperactivate JNK, which in turn phosphorylates BCL-XL and induces a dependency on MCL-1 to neutralize BIM. Accumulation of BIM bound to MCL-1 effectively primes cells for apoptosis, rendering cells sensitive to the MCL-1 BH3 mimetic AMG 176. These results suggest loss of LKB1 results in an inducible vulnerability in *KRAS*-mutant lung cancers and may serve as a genomic biomarker to guide patient selection for $KRAS^{G12C}$ + MCL-1 combination therapy.

RESULTS

LKB1 loss confers sensitivity to combined MAPK + MCL-1 inhibition in *KRAS*-mutant NSCLC models

To assess the combined activity of $KRAS^{G12C}$ + MCL-1 inhibitors in $KRAS^{G12C}$-mutant NSCLC, we screened a panel of $KRAS^{G12C}$-mutant NSCLC cell lines harboring diverse co-occurring mutations (Fig. S1A) with sotorasib alone or in combination with AMG 176. Consistent with prior studies of $KRAS^{G12C}$ inhibitors (Canon *et al.*, 2019; Hallin et al., 2020; Janes et al., 2018; Misale *et al.*, 2019), we observed varying sensitivity to single-agent $KRAS^{G12C}$ inhibition, which was independent of the most common co-occurring mutations such as *TP53*, *STK11*/LKB1 and *KEAP1* (Fig. S1B-E; Sup Table 1). The combination of sotorasib with AMG 176 led to greater suppression of cell viability than single-agent sotorasib in some cell lines (Fig. 1A), although the additive effect was variable across the cell line panel (Fig. 1B). To quantify the efficacy of co-targeting MCL-1 and $KRAS^{G12C}$ compared to $KRAS^{G12C}$ alone, we calculated the relative change in AUC (e.g., the area between the single agent and combination dose response curves, normalized to the effect of sotorasib alone), referred to hereafter as simply ΔAUC (Fig. S2A). We observed the greatest combination activity in cell lines with co-occurring mutations in *STK11*/loss of LKB1 (Fig. 1B, D). To extend this finding to NSCLC cell lines with *KRAS* mutations other than G12C (for which KRAS inhibitors are not yet clinically available), we examined the MEK inhibitor trametinib in combination with AMG 176 (or the related compound AM-8621) (Nangia *et al.*, 2018). Similarly, we observed greater combination activity of trametinib + AMG 176 in cell lines with LKB1 loss (Fig. 1C, D). To confirm that this effect was due to enhanced induction of apoptosis, we assessed the apoptotic response of cells with high or low ΔAUC values to trametinib + AMG 176 or either drug alone. Consistent with the effect on viability, LKB1-deficient cell lines with high ΔAUC values exhibited robust apoptosis after treatment with trametinib + AMG 176, while the apoptotic response of LKB1 wild-type (WT) cell lines was minimal (Fig. 1E).

To test whether LKB1 status plays a causal role in determining the sensitivity of *KRAS*-mutant NSCLC cells to combined $KRAS^{G12C}$ or MEK (e.g., MAPK pathway) + MCL-1 inhibition, we restored LKB1 expression in LKB1-deficient cell lines (Fig. S2B). We observed that re-expression of LKB1 decreased sensitivity to combined sotorasib or trametinib + MCL-1 inhibition (Fig. 1F-H, Fig. S2B, S2D). Conversely, CRISPR-mediated deletion of LKB1 sensitized LKB1 WT cells to sotorasib or trametinib + MCL-1 inhibition (Fig. 1F-H, S2C-D). Restoration or deletion of LKB1 did not alter the response to sotorasib alone (Fig. S2E), suggesting that the changes in sensitivity to the drug combination that occur upon gain or loss of LKB1 are mediated primarily by differences in MCL-1-dependent regulation of apoptosis. Consistent with this notion, restoration or deletion of LKB1 decreased or increased the apoptotic response to trametinib + AMG 176, respectively (Fig. 1I). To confirm these results *in vivo*, we established isogenic H2030 EV (empty vector pBabe) and LKB1 xenograft tumors in mice. Similar to the *in vitro* results, restoration of LKB1 abolished tumor regression of H2030 xenograft tumors in response to sotorasib or trametinib + AMG 176

bioRxiv preprint doi: https://doi.org/10.1101/2022.09.29.510137; this version posted September 30, 2022. The copyright holder for this preprint (which was not certified by peer review) is the author/funder, who has granted bioRxiv a license to display the preprint in perpetuity. It is made available under aCC-BY-NC-ND 4.0 International license.

(Fig. 1J, S2F). Collectively, these results demonstrate that that loss of LKB1 sensitizes *KRAS*-mutant NSCLC cells to combined MAPK + MCL-1 inhibition both *in vitro* and *in vivo*.

JNK activation in LKB1-deficient cells underlies sensitivity to MCL-1 inhibition

LKB1 is a master serine/threonine kinase that regulates multiple cellular process including growth (Inoki et al., 2003; Shaw et al., 2004a), cell metabolism (Jeon et al., 2012; Nakada et al., 2010) and cell polarity (Baas et al., 2004; Barnes et al., 2007; Shelly et al., 2007). We hypothesized that loss of LKB1 rewires downstream kinase signaling networks to confer dependency on MCL-1 in the setting of KRAS or MEK inhibition. Supporting this, expression of kinase-dead LKB1^{K781} (kd) mutant (Shaw et al., 2004b) did not rescue LKB1-deficient cells from combined MEK + MCL-1 inhibition (Fig. S3A, B), demonstrating that LKB1 catalytic activity is required for the observed difference in drug sensitivity. To identify differences in kinase signaling in *KRAS*-mutant NSCLC cells with or without *LKB1*, we performed mass spectrometry-based global phosphoproteome profiling (Kreuzer et al., 2019) of isogenic H2030 (EV, LKB1 and LKB1-kd) and H358 (KO GFP, KO LKB1) cells before and after treatment with trametinib (Fig. 2A). We quantified 27364 unique phosphosites (Fig. S3C-D), then performed phosphosites signature analysis (Krug et al., 2019) to identify the kinases that were differentially activated in each of these contexts. Consistent with the known effect of MEK inhibition on cell cycle progression (Pumiglia and Decker, 1997), we observed down-regulation of cell cycle associated phospho-signatures including cyclin-dependent kinases, ATM, ATR, Aurora Kinase B, and PLK1 in response to trametinib treatment (Fig. S3E). In the absence of drug treatment, there were few differences (and no overlap) in kinase signatures between LKB1 wild-type and deficient cells (Fig. S3F), likely a result of the nutrient-rich cell culture environment.

To identify drug-induced differences in kinase activity regulated by LKB1, we looked for kinase phospho-signatures that were enriched in trametinib-treated LKB1-deficient cells relative to their wild-type counterparts (H2030 EV versus LKB1, H358 KO LKB1 versus KO GFP) but not enriched in H2030 EV versus kinase-dead LKB1^{K87I} cells (Fig. 2A). While several signatures were enriched in trametinib-treated LKB1-deficient cells for either isogenic pair, only one signature – JNK1 – satisfied these criteria (Fig. 2B, S3G). Specifically, the phosphorylation of well-established substrates of JNK1, such as ATF2, JUN and JUNB, increased to a greater extent in H2030 EV and H358 KO LKB1 cells after trametinib treatment compared to their LKB1 wild-type pairs (Fig. S3H). To confirm these results, we examined JNK Thr183/Tyr185 phosphorylation in H2030 and H358 isogenic pairs. Combined sotorasib or trametinib + AMG 176 treatment led to a time-dependent increase in JNK phosphorylation in H2030 EV cells, which could be suppressed by knockdown of MKK7, which phosphorylates and activates JNK (Fig. S4A). Re-expression of LKB1 suppressed JNK phosphorylation in H2030 cells, and conversely, deletion of LKB1 in H358 cells led to increased phospho-JNK after drug treatment (Fig. 2C-D). We extended these findings by comparing the induction of phospho-JNK across a larger cohort of *KRAS*-mutant NSCLC cells treated with trametinib + AMG 176. Despite an expected degree of heterogeneity between cell lines, we observed that cell lines with LKB1 loss in general exhibited greater induction of JNK phosphorylation compared to cell lines with wild-type LKB1 (Fig. 2E, S4B). Corroborating the results in H2030 cells, re-expression of LKB1 in H23 cells blunted the induction of phospho-JNK in response to trametinib + AMG 176 (Fig. S4C).

These data suggest that LKB1 suppresses JNK-dependent stress signaling that occurs upon inhibition of MAPK pathway signaling. c-Jun N-terminal kinases (JNKs) modulate cell proliferation, differentiation and survival in response a number of different environmental and cellular stressors (Wagner and Nebreda, 2009). To examine whether hyperactivation of JNK signaling in LKB1-deficient cells is specific to MAPK inhibition or reflects a more general role for regulation of JNK

bioRxiv preprint doi: https://doi.org/10.1101/2022.09.29.510137; this version posted September 30, 2022. The copyright holder for this preprint (which was not certified by peer review) is the author/funder, who has granted bioRxiv a license to display the preprint in perpetuity. It is made available under aCC-BY-NC-ND 4.0 International license.

by LKB1, we exposed H2030 EV or LKB1 cells to UV light, a well-established inducer of JNK signaling (Derijard et al., 1994; Hibi et al., 1993). We observed an increase in phospho-JNK in H2030 EV cells that peaked within 60 minutes, which was reduced in H2030 LKB1 cells (Fig. S4D). This suggests that LKB1 may play a general role in suppressing JNK stress signaling in response to a variety of stimuli.

To test whether JNK activation underlies the increased sensitivity of LKB1-deficient *KRAS*-mutant cancer cells to combined MAPK + MCL-1 inhibition, we used siRNA to simultaneously knock down both JNK1 and 2 isoforms (Fig. S4E) and assessed the response to combined sotorasib or trametinib + AMG 176. While JNK1/2 knockdown had little effect on sensitivity to trametinib alone, JNK1/2 depleted cells exhibited reduced sensitivity to both drug combinations, phenocopying the effect of LKB1 re-expression (Fig. 4F-G, S4F). Collectively, these results suggest that hyper-activation of JNK signaling in the absence of LKB1 increases the MCL-1 dependence of LKB1-deficient *KRAS*-mutant NSCLC cells and sensitizes them to combined $KRAS^{G12C}$ or MEK + MCL-1 inhibition.

Suppression of JNK activation by LKB1 is mediated by NUAK kinases

LKB1 exerts its effects via phosphorylation and activation of multiple members of the AMP-activated protein kinase (AMPK) family. For instance, LKB1 plays a central role in energy homeostasis by sensing increased intracellular AMP/ATP ratio and phosphorylating AMPK, which in turn suppresses energy consumption by inhibiting mTOR and stimulating autophagy (Shackelford and Shaw, 2009). Recently, the AMPK-related SIK kinases have been shown to play a major role in mediating the suppressive effects of LKB1 on tumorigenesis and metastatic potential in models of *KRAS*-mutant NSCLC (Hollstein et al., 2019; Murray et al., 2019). However, how LKB1 regulates apoptotic priming is largely unknown. To identify the LKB1 substrate kinase(s) that mediate the suppressive effect of LKB1 on drug-induced JNK activation and MCL-1 dependency, we simultaneously silenced the expression of multiple members within each AMPK-related kinase family that are expressed in NSCLC (Murray *et al.*, 2019) (Fig. 3A, S5A-D). Silencing NUAK1+2 was sufficient to restore the sensitivity of H2030 LKB1 cells to combined sotorasib or trametinib + AMG 176 to a similar level as LKB1-deficient H2030 cells (Fig. 3B-C, S5E). In contrast, silencing SIKs, AMPKs or MARKs in the context of LKB1 re-expression did not restore drug sensitivity (Fig. 3B, S5F). In addition, we observed a similar difference in drug sensitivity between LKB1-deficient and LKB1-restored cells when cultured in high or low/absent glucose conditions (Fig. S5G), consistent with a nutrient-independent mechanism. Knockdown of NUAK1/2 restored drug-induced JNK phosphorylation in H2030 cells expressing LKB1 to a similar level as H2030 control cells (Fig. 3D). Collectively, these results suggest that loss of LKB1-NUAK1/2 signaling leads to increased JNK signaling and sensitivity to combined MAPK + MCL-1 inhibition.

JNK activation modulates interactions between BCL-2 family proteins to drive an MCL-1 dependent state

Inhibition of MEK/ERK signaling leads to BIM accumulation and increases apoptotic priming in oncogene-driven cancers treated with various targeted therapies, driving cells into an MCL-1 and/or BCL-XL dependent state (Cragg *et al.*, 2009) (Hata *et al.*, 2015). To investigate how LKB1 modulates MCL-1 dependence, we performed BH3 profiling (Montero et al., 2015) (Fraser et al., 2019; Ni Chonghaile et al., 2011) to detect changes in mitochondrial sensitivity to various pro-apoptotic stimuli in isogenic LKB1-deficient or wild-type cell lines before and after treatment with trametinib (Fig. 4A). As expected, trametinib treatment increased overall apoptotic priming (Fig. S6A). Trametinib induced a greater increase in MCL-1 dependence (expressed as "Δpriming") in

bioRxiv preprint doi: https://doi.org/10.1101/2022.09.29.510137; this version posted September 30, 2022. The copyright holder for this preprint (which was not certified by peer review) is the author/funder, who has granted bioRxiv a license to display the preprint in perpetuity. It is made available under aCC-BY-NC-ND 4.0 International license.

LKB1-deficient compared to LKB1 wild-type cells (Fig. 4B, S6B). Re-expression of LKB1 in LKB1-deficient cell lines suppressed trametinib-induced MCL-1 apoptotic priming, while BCL-XL priming was largely unaffected (Fig. 4B, S6C). Conversely, deletion of LKB1 in H358 cells increased trametinib-induced MCL-1 dependency as well as BCL-XL dependency. To investigate the basis for increased MCL-1 dependent priming in LKB1-deficient cells, we examined MCL-1 protein expression levels, as this is highly dependent on cap-dependent translational regulated by mTOR (which is regulated by AMPK). There was no correlation between MCL-1 or BCL-XL protein expression and LKB1 status in *KRAS*-mutant NSCLC cell lines (Fig. S6D-E) or isogenic cell line pairs (for example, see Fig. S7B), again consistent with an AMPK- and nutrient-independent effect of LKB1. Next, we examined interactions between BIM and MCL-1 or BCL-XL. Co-immunoprecipitation (Co-IP) experiments revealed increased BIM bound to MCL-1 and BCL-XL after trametinib treatment (Fig. 4C), in line with prior studies (Nangia *et al.*, 2018). LKB1-deficient cells treated with trametinib had a greater amount of BIM bound to MCL-1, and less BIM bound to BCL-XL, compared to LKB1 wild-type cell lines (Fig. 4D, S7A-B). Restoration of LKB1 in deficient cell lines reduced the amount of BIM bound to MCL-1 after trametinib treatment, and knocking out LKB1 in wild-type cells increased the amount of BIM bound to MCL-1 (Fig. 4E-F, S7C-D). Notably, except for one cell line (A427), we did not observe an impact of LKB1 re-expression/knock-down on baseline BIM:MCL-1 binding in the absence of drug treatment (Fig. 4F, S7D). These results indicate that loss of LKB1 promotes the formation of BIM:MCL-1 complexes in the context of MAPK inhibition, functionally inducing an MCL-1 dependent state and priming AMG 176 sensitivity.

MCL-1 and BCL-XL can be phosphorylated at multiple residues by numerous kinases, including JNK and ERK, leading to context-specific and divergent effects on protein stability/degradation, BIM binding affinity and apoptosis (Morel et al., 2009) (Inoshita et al., 2002) (El Fajoui et al., 2011; Follis et al., 2018; Kharbanda et al., 2000; Pan et al., 2017). MCL-1 phosphorylation at T163 decreased acutely upon trametinib treatment consistent with a loss of ERK phosphorylation (Domina et al., 2004) and then rebounded at later time points coinciding with activation of JNK (Fig. S8A). Restoration of LKB1 in LKB1-deficient cells reduced the rebound in MCL-1 phosphorylation, while silencing LKB1 in wild-type cells increased MCL-1 phosphorylation (Fig. S8A-B). Trametinib treatment also induced phosphorylation of BCL-XL at S62 in LKB1-deficient cells at later time points, which was suppressed by re-expression of LKB1 (Fig. S8A). Notably, the combination of trametinib with AMG 176 induced rapid phosphorylation of BCL-XL. Restoration of LKB1 reduced BCL-XL S62 phosphorylation, while knocking out LKB1 increased BCL-XL S62 phosphorylation (Fig. 5A). Silencing JNK1/2 expression reduced drug-induced phosphorylation of both MCL-1 and BCL-XL to a similar level as the corresponding LKB1-restored isogenic cell line (Fig. 5B, compare lanes 3, 4 and 7).

To assess whether JNK-mediated phosphorylation of MCL-1 and BCL-XL impacts drug sensitivity, we expressed DOX-inducible MCL-1 or BCL-XL phosphorylation-site mutants in H2030 cells while simultaneously knocking down expression of endogenous MCL-1 or BCL-XL (Fig. 5C, S8C-F). While mutating MCL-1 phosphorylation sites to alanine had little effect on sensitivity to trametinib + AMG 176 (Fig 5D, S8G), expression of the BCL-XL S62A mutant reduced sensitivity to both sotorasib or trametinib + AMG 1767 (Fig 5E-G), phenocopying LKB1 re-expression and JNK1/2 knockdown. Conversely, the BCL-XL S62E phosphomimetic increased the sensitivity of H2030 LKB1 cells (Fig. 5H). These results suggest that the increased MCL-1 dependency of LKB1-deficient cells is mediated by BCL-XL phosphorylation. Prior studies have demonstrated that sensitivity of cancer cells to MCL-1 inhibition is inversely related to BCL-XL expression level and the capacity for BCL-XL to neutralize pro-apoptotic BH3 proteins such as BIM (Kotschy et al., 2016) (Caenepeel et al., 2018). Phosphorylation of BCL-XL S62 induces a conformational change in which a dysregulated domain folds into the BCL-XL BH3 binding groove to prevent BIM binding

bioRxiv preprint doi: https://doi.org/10.1101/2022.09.29.510137; this version posted September 30, 2022. The copyright holder for this preprint (which was not certified by peer review) is the author/funder, who has granted bioRxiv a license to display the preprint in perpetuity. It is made available under aCC-BY-NC-ND 4.0 International license.

(Follis *et al.*, 2018). Therefore, we hypothesized that phosphorylation of BCL-XL S62 by JNK compromises the ability of BCL-XL to sequester BIM that is liberated from MCL-1 upon MCL-1 inhibition. To test this hypothesis, we studied the dynamics of BIM:MCL-1 and BIM:BCL-XL interactions by first treating cells with trametinib to increase BIM bound to MCL-1, then treating with a short pulse of AMG 176 and assessing the ability for BCL-XL to sequester BIM released from MCL1 (Fig. 6A). In LKB1-deficient H2030 cells, very little BIM was sequestered by BCL-XL upon treatment with AMG 176, compared to LKB1 wild-type SW1573 cells, which exhibited substantial sequestration of BIM by BCL-XL (Fig. 6B). Restoring LKB1 expression or silencing JNK1/2 in H2030 cells increased the amount of BIM sequestered by BCL-XL after addition of AMG 176 (Fig. 6C-D). In H2030 EV cells, the BCL-XL S62A mutant exhibited increased BIM:BCL-XL binding, whereas in H2030 LKB1 cells, the phospho-mimetic S62E mutant decreased BIM:BCL-XL binding (Fig. 6E). Knock-down of NUAK1/2 expression in H2030 cells, which we showed restored drug-induced JNK phosphorylation (Fig. 3D), restored the drug-induced phosphorylation of BCL-XL S62 (Fig. 6F). Collectively, these results demonstrate that in the context of LKB1 loss, inhibition of MEK/ERK signaling leads to activation of JNK, which in turn creates an MCL-1 dependent state by phosphorylating BCL-XL and decreasing its capacity to buffer the pro-apoptotic effects of BIM (Fig. 6G).

LKB1 loss predicts sensitivity to KRAS^{G12C} + MCL-1 inhibition in *KRAS*-mutant NSCLC PDX tumors and patient tumor explants

To investigate the clinical relevance of our findings, we performed BH3 profiling on *KRAS*^{G12C}-mutant NSCLCs (solid tissue metastatic lesions or tumor cells isolated from malignant pleural effusions) after ex vivo exposure to sotorasib or trametinib (Fig. 7A). For MGH1196, which harbored a co-occurring STK11/LKB1 mutation, both sotorasib and trametinib treatment increased MCL-1 dependence (MS1 peptide), but not BCL-XL priming (HRK peptide) (Fig. 7B). Consistent with this effect, co-immunoprecipitation experiments performed on tumor cells isolated from a malignant pleural effusion obtained from the same patient revealed drug-induced increases in BIM bound to MCL1 (Fig. 7C). In contrast, LKB1 wild-type MGH9348 and MGH10191 tumor cells exhibited no MCL-1 dependent priming after *ex vivo* drug treatment. To extend these findings, we performed BH3 profiling on *KRAS*-mutant (G12C and other) NSCLC patient-derived xenograft (PDX) models with or without co-occurring LKB1 loss after short-term treatment with trametinib. Similar to the patient tumors and in vitro cell line models, LKB1-deficient tumors exhibited increased MCL-1-dependent priming compared to tumors with wild-type LKB1 (Fig 7D). Longer treatment of mice bearing *KRAS*^{G12C}-mutant NSCLC PDX tumors demonstrated that addition of AMG 176 to sotorasib resulted in greater tumor response in LKB1-deficient but not LKB1 wild-type models (Fig. 7E, S7A-E). Thus, LKB1 loss is associated with increased MCL-1 dependence upon treatment with sotorasib or trametinib in clinical *KRAS*^{G12C}-mutant NSCLC tumors and PDX models, creating an apoptotic vulnerability that can be exploited by concurrent inhibition of MCL-1.

DISCUSSION

As increasing numbers of KRAS^{G12C} inhibitor drug combinations enter the clinic, the identification of specific vulnerabilities conferred by recurrent co-occurring mutations is of considerable interest, as it may enable the development of biomarker-driven combination therapies with enhanced activity in distinct subsets of patients. Prior studies have demonstrated that pro-survival BCL-2 family proteins such as BCL-2, BCL-XL and MCL-1 can oppose oncogene-directed targeted therapies by sequestering pro-apoptotic BIM that accumulates upon suppression of MEK/ERK signaling. BH3 mimetic drugs that block these interactions can sensitize cells to targeted therapies;

bioRxiv preprint doi: https://doi.org/10.1101/2022.09.29.510137; this version posted September 30, 2022. The copyright holder for this preprint (which was not certified by peer review) is the author/funder, who has granted bioRxiv a license to display the preprint in perpetuity. It is made available under aCC-BY-NC-ND 4.0 International license.

however, individual tumors of a given cancer type may rely on one or more different BCL-2 family proteins (predominantly BCL-XL and MCL-1 in solid malignancies) (Corcoran *et al.*, 2013; Nangia *et al.*, 2018). Although sensitivity to BH3 mimetics has been shown to inversely correlate with the expression level of compensatory BCL-2 family proteins (i.e., high expression of MCL-1 correlates with decreased sensitivity to BCL-XL inhibitors and vice versa), no genomic biomarkers have been identified that can reliably predict the specific apoptotic dependency of a given tumor. Our finding that *KRAS*-mutant NSCLCs with co-occurring mutations or loss of LKB1 become dependent on MCL-1 when KRAS or downstream MEK signaling is inhibited represents a step toward this goal, revealing a vulnerability that can be therapeutically exploited by combining $KRAS^{G12C}$ or MEK inhibitors with BH3 mimetic MCL-1 inhibitors.

Using a large panel of genetically-defined *KRAS*-mutant NSCLC models, we observed an unexpected correlation between LKB1 loss and MCL-1 dependence specifically in the context of $KRAS^{G12C}$ or MEK inhibition, independent of variation in MCL-1 or BCL-XL expression levels. Genetic manipulation of LKB1 (re-expression or gene deletion) altered the sensitivity of isogenic models to combined MCL-1 + KRAS or MEK inhibition *in vitro* and *in vivo*, demonstrating that LKB1 plays a critical role in determining apoptotic dependencies in this context. Mechanistically, in LKB1-deficient cells, KRAS or MEK inhibition leads to hyperactivation of JNK1/2, which phosphorylates BCL-XL and diminishes its capacity to bind and sequester BIM. In LKB1 wild-type cells, LKB1 suppresses JNK activation via its phosphorylation of the AMPK-related NUAK kinases. LKB1-deficient cells exhibited a compensatory increase in BIM binding to MCL-1, indicating that in the absence of MCL-1 inhibition, they maintain the capacity to buffer excess BIM induced by KRAS or MEK inhibition. Indeed, we did not observe any difference in sensitivity of LKB1-mutant and wild-type cell lines to sotorasib alone, and early clinical results have shown that LKB1 mutant and LKB1 wild-type patients have equivalent response rates to sotorasib or adagrasib (Janne *et al.*, 2022; Skoulidis *et al.*, 2021). However, the increased reliance of LKB1-deficient cells on MCL-1 to buffer the increase in BIM induced by KRAS or MEK inhibition results in accumulation of BIM:MCL-1 complexes and effectively primes *KRAS*-mutant LKB1-deficient NSCLCs for apoptosis upon inhibition of MCL-1 and release of BIM.

JNK has been reported to modulate apoptotic signaling by phosphorylating multiple pro- and anti-apoptotic BCL-2 family members, including BIM (Becker et al., 2004; Corazza et al., 2006; Hubner et al., 2008; Lei and Davis, 2003), BAX (Park et al., 2014; Robitaille et al., 2008; Tsuruta et al., 2004), BCL-XL (El Fajoui *et al.*, 2011; Kharbanda *et al.*, 2000) and MCL-1 (Mazumder et al., 2012; Morel *et al.*, 2009; Pan *et al.*, 2017; Tong et al., 2018). The consequences of differential phosphorylation are complex and can impact both protein stability/turnover as well as protein-protein interactions, leading to both pro- and anti-apoptotic effects in a context-specific manner. While a number of studies have examined the impact of JNK phosphorylation of apoptotic proteins in response to TNFα- and TRAIL-induced apoptosis (Corazza *et al.*, 2006; El Fajoui *et al.*, 2011; Inoshita *et al.*, 2002; Morel *et al.*, 2009; Park *et al.*, 2014; Yuan et al., 2017), less is known about the role of JNK in modulating apoptosis in response to inhibition of growth factor signaling pathways. While we observed JNK-mediated phosphorylation of both MCL-1 and BCL-XL in response to KRAS and MEK inhibition, elimination of JNK phosphorylation sites only in BCL-XL but not MCL-1 phenocopied the decrease in MCL-1 dependence observed with JNK knockdown or LKB1 re-expression. Future studies will be necessary to determine whether JNK phosphorylation of MCL-1 may confer apoptotic vulnerabilities in other therapeutic contexts.

Inactivating mutations or loss of STK11/LKB1, which occur in about 30% of the *KRAS*-mutant NSCLC (Cancer Genome Atlas Research, 2014; Jordan et al., 2017), define one of the major genomic sub-groups recently defined by Skoulidis and colleagues (KP – *TP53* loss, KL – *STK11*/LKB1 loss, KC – *CDKN2A/B* inactivation) (Skoulidis et al., 2015). *KRAS*-mutant NSCLCs

bioRxiv preprint doi: https://doi.org/10.1101/2022.09.29.510137; this version posted September 30, 2022. The copyright holder for this preprint (which was not certified by peer review) is the author/funder, who has granted bioRxiv a license to display the preprint in perpetuity. It is made available under aCC-BY-NC-ND 4.0 International license.

with co-occurring LKB1 loss have received particular attention recently because of reduced responsiveness to immune checkpoint blockade (Ricciuti et al., 2022; Skoulidis *et al.*, 2018) and poor overall prognosis (Rosellini et al., 2022). LKB1 is a master kinase that regulates diverse cellular processes including cell proliferation, polarity, metabolism and development via phosphorylation of multiple members of AMPK family kinases (Kullmann and Krahn, 2018; Shackelford and Shaw, 2009). In particular, the role of LKB1 in regulating energy homeostasis via AMPK has been well defined. In settings of energy stress (high AMP:ATP ratio), AMPK limits anabolic processes by inhibiting mTORC1 through TSC2 (Van Nostrand et al., 2020). Interestingly, expression levels of MCL-1 are highly dependent upon mTOR-mediated cap-dependent translation, and inhibition of mTOR by small-molecule inhibitors has been shown to reduce MCL-1 expression and confer apoptotic sensitivity (Faber et al., 2014). Although this suggests a potential link between LKB1 loss and MCL-1 dependency via the AMPK-mTOR axis, we did not observe any change in MCL-1 expression upon re-expression or deletion of LKB1 in LKB1-deficient and wild-type cells, respectively. Moreover, silencing AMPK expression did not phenocopy the effect of LKB1 loss on MCL-1 inhibitor sensitivity. Activation of AMPK by LKB1 leads to a number of other metabolic effects including a switch from glycolysis to mitochondrial respiration (Pooya et al., 2014), reduced fatty acid synthase through inhibition of ACC1 and 2 (Jeon *et al.*, 2012), induction of autophagy through ULK1 (Egan et al., 2011) and mitochondrial biosynthesis via PGC-1 (Gan et al., 2010). LKB1 loss in cancers can lead to mitochondrial defects (Shackelford et al., 2013) and energetic and redox stress characterized by decreased ATP, NADPH/NADP ratio and increased reactive oxygen species (Galan-Cobo et al., 2019; Ji *et al.*, 2007; Li et al., 2015). Accumulation of ROS can trigger senescence, apoptosis or ferroptosis (Hayes et al., 2020), raising the possibility that LKB1 loss could facilitate apoptosis through increased cellular ROS. However, we did not observe a change in intracellular ROS upon restoration or deletion of LKB1 in our isogenic models (data not shown), nor did altering NADP/NADPH ratio (Cracan et al., 2017) change the sensitivity to MCL-1 inhibition (data not shown). Collectively, these results support an AMPK-independent mechanism by which LKB1 modulates JNK signaling and MCL-1 dependency.

Beyond its role regulating metabolism via AMPK, LKB1 loss promotes tumorigenesis by reprogramming epigenetic states, facilitating lineage plasticity and promoting metastasis (Ji *et al.*, 2007; Li *et al.*, 2015; Murray et al., 2022; Pierce et al., 2021; Zhang et al., 2017). Recent studies have revealed a central role for the AMPK-related SIK kinases in mediating the suppressive effects of LKB1 on tumorigenesis (Hollstein *et al.*, 2019; Murray *et al.*, 2019) . The role of other AMPK-related kinases in mediating the tumor suppressor effects of LKB1 are not well defined. NUAK kinases have been shown to regulate cellular polarity, adhesion and cell cycle in normal tissues (Amin et al., 2009; Banerjee et al., 2014; Zagorska et al., 2010) and to play a critical role in neurite formation (Blazejewski et al., 2021). Our results reveal that NUAKs can function as negative regulators of JNK signaling, although further investigation will be required to define the intermediate steps linking NUAK1/2 to JNK. To our knowledge, the LKB1/NUAK/JNK axis represents a novel mechanism by which LKB1 suppresses JNK stress signaling and regulates apoptosis. While our study focused on *KRAS*-mutant lung cancers treated with KRAS or MEK inhibitor targeted therapies, we also provide evidence that LKB1 suppresses JNK activation in response to UV radiation, suggesting a fundamental role for LKB1 in regulating JNK stress signaling in response to a variety of stimuli. From an evolutionary perspective, we speculate that the ability for LKB1 to suppress JNK signaling may be advantageous in normal tissues facing energy or redox stress by temporarily suppressing apoptosis until compensatory mechanisms (also regulated by LKB1) can be engaged. It is less clear whether modulation of JNK signaling contributes to the tumor suppressor functions of LKB1, or whether the ability to hyperactivate JNK signaling provides an advantage to cancer cells with loss of LKB1. It is important to note that the differential JNK activation and increase in MCL-1 dependency conferred by LKB1 loss was only

bioRxiv preprint doi: https://doi.org/10.1101/2022.09.29.510137; this version posted September 30, 2022. The copyright holder for this preprint (which was not certified by peer review) is the author/funder, who has granted bioRxiv a license to display the preprint in perpetuity. It is made available under aCC-BY-NC-ND 4.0 International license.

observed in the setting of MAPK inhibition, suggesting that the functional effects of this pathway may only be unmasked in specific contexts in response to select perturbations.

In summary, we identify a novel mechanism by which LKB1 regulates JNK stress signaling and modulates apoptotic dependencies in *KRAS*-mutant NSCLCs. In response to KRAS or MEK inhibition, LKB1-deficient cells exhibit hyperactivation of JNK and increased reliance on MCL-1 to buffer the increase in BIM. While LKB1-deficiency does not confer increased sensitivity to $KRAS^{G12C}$ or MEK inhibitors used as single agents, they become primed for apoptosis upon treatment with MCL-1 BH3 mimetics. These results provide rationale for the clinical development of combined $KRAS^{G12C}$ + MCL-1 inhibitors and suggest a biomarker-informed approach based on mutations or genomic loss of *STK11*/LKB1.

bioRxiv preprint doi: https://doi.org/10.1101/2022.09.29.510137; this version posted September 30, 2022. The copyright holder for this preprint (which was not certified by peer review) is the author/funder, who has granted bioRxiv a license to display the preprint in perpetuity. It is made available under aCC-BY-NC-ND 4.0 International license.

METHODS

Cell culture

Publicly-available *KRAS-mutant* NSCLC cell lines were obtained from the Center for Molecular Therapeutics at the Massachusetts General Hospital (MGH) Cancer Center and STR validation was performed at the initiation of the project (Biosynthesis, Inc.). Cell lines were routinely tested for mycoplasma during experimental use. Cell lines were maintained in RPMI supplemented with 5% FBS except A427, SW1573, H2009, H1573, which were maintained in DMEM/F12 supplemented with 5% FBS. Patient-derived NSCLC cell lines were established in our laboratory from surgical resections, core-needle biopsies, or pleural effusion samples as previously described (41), with the exception of the MGH1070 cell line, which was derived from a primary mouse PDX model. All patients signed informed consent to participate in a Dana- Farber/Harvard Cancer Center Institutional Review Board–approved protocol, giving permission for research to be performed on their samples. Clinically observed *KRAS* mutations (determined by MGH SNaPshot NGS genotyping panel) were verified in established cell lines. Established patient-derived cell lines were maintained in RPMI + 10% FBS.

Cell viability assessment

Cell viability was assessed using the CellTiter-Glo assay (Promega). Cells were seeded into 96-well plates 24 hours prior to drug addition, and cell proliferation was determined 72 hours after addition of drug by incubating cells with CellTiter-Glo reagent (50 µL/well) for 30 minutes on a shaking platform at room temperature. Luminescence was quanitified using a SpectraMax i3x plate reader (MolecularDevices).

PI/Annexin apoptosis assay

Cells were seeded in triplicate at low density 24 hours prior to drug addition. Seventy-two hours after adding drugs, floating and adherent cells were collected and stained with propidium iodide (PI) and Cy5-Annexin V (BD Biosciences) and analyzed by flow cytometry. The annexin-positive apoptotic cell fraction was quantified using FlowJo software.

Generation of engineered cell lines

EV and LKB1 cell lines: EV (pBabe) and LKB1 retro-viral vectors were gifts from Dr. Kwok-Kin Wong (NYU). EV and LKB1 virus were prepared by transfecting HEK293 cells with EV or LKB1, VSV-G (Addgene #8454), Gag-Pol (Addgene #14887) using Lipofectamine 3000 (ThermoFisher) and collecting viral particles in the supernatant. Stable cell lines were generated by infecting *KRAS*-mutant NSCLC lines with EV or LKB1 virus followed by puromycin selection.

LKB1 knock-out cell lines: sgRNAs targeting the *STK11* locus were designed using CHOP-CHOP and cloned into pSpCas9(BB)-2A-GFP (Addgene #48138). *KRAS*-mutant NSCLC cell lines were transiently transfected with the plasmids and sorted for single clone formation by FACs. After clonal expansion, 20 clones were selected and loss of LKB1 expression was assessed by western blot. Alternatively, LKB1 sgRNAs were cloned into lentiCRISPR v2 (Addgene #52961). Lentiviral particles were prepared by transfecting HEK293 cells with EV or sgLKB1, VSV-G (Addgene #8454) and Δ8.91 using Lipofectamine 3000 (ThermoFisher). Stable cell lines were generated by infecting *KRAS*-mutant NSCLC lines with lentiCRISPR v2 or sgLKB1 virus followed by blasticidin selection.

DOX-inducible MCL-1, BCL-XL cell lines: Full length wild-type or mutant MCL-1, BCL-XL coding sequences were synthesized (GenScript) and cloned into pInducer20 (gift from Lee Zou, MGH). Lentiviral particles were prepared by transfecting HEK293 cells with pInducer20 or pInducer20-MCL-1/ pInducer20-BCL-XL, VSV-G (Addgene #8454) and Δ8.91 using Lipofectamine 3000 (ThermoFisher). Stable cell lines were generated by infecting *KRAS*-mutant NSCLC lines were infected with EV or sgLKB1 virus followed by selection with neomycin/G418.

bioRxiv preprint doi: https://doi.org/10.1101/2022.09.29.510137; this version posted September 30, 2022. The copyright holder for this preprint (which was not certified by peer review) is the author/funder, who has granted bioRxiv a license to display the preprint in perpetuity. It is made available under aCC-BY-NC-ND 4.0 International license.

Mouse xenograft studies

All animal studies were conducted through Institutional Animal Care and Use Committee–approved animal protocols in accordance with institutional guidelines. *KRAS-mutant* NSCLC PDX models were generated from surgical resections, core-needle biopsies, or pleural effusion samples by subcutaneous implantation into NSG mice (Jackson Labs). Subcutaneous tumors were serially passaged twice to fully establish each model. Clinically observed *KRAS* mutations were verified in each established model. For drug studies, PDX tumors were directly implanted subcutaneously into NSG or athymic nude (NE/Nu) mice and allowed to grow to 250 to 400 mm^3. For H2030 xenograft studies, cell line suspensions were prepared in 1:1 matrigel:PBS, and 5 × 10^6 cells were injected unilaterally into the subcutaneous space on the flanks of athymic nude (Nu/Nu) mice and allowed to grow to approximately 350 mm^3. Tumors were measured with electronic calipers, and the tumor volume was calculated according to the formula $V = 0.52 \times L \times W^2$. Mice with established tumors were randomized to drug treatment groups using covariate adaptive randomization to minimize differences in baseline tumor volumes. Trametinib was dissolved in 0.5% HPMC/0.2% Tween 80 (pH 8.0) and administered by oral gavage daily at 3 mg/kg, 6 days per week. Sotorasib was dissolved in 2% HPMC/0.1% Tween 80 (pH 7) and administered by oral gavage daily at 100 mg/kg, 6 days per week. AMG 176 was dissolved in 25% hydroxypropylbeta- cyclodextrin (pH8.0) and administered by oral gavage daily 50 mg/kg.

Quantitative RT-PCR analysis

RNA was extracted using the Qiagen RNeasy kit. cDNA was prepared with the Transcriptor High Fidelity cDNA Synthesis Kit (Roche) using oligo-dT primers. Quantitative PCR was performed with gene specific primers (Supplemental table 2) using SYBR™ Select Master Mix (Applied biosystem) on a Lightcycler 480 (Thermofisher). Relative gene expression was calculated by using the Δ ΔCT method by normalizing to *ACTB*.

Western Blot analysis

Cells were seeded in either 6-well or 6 cm plates and drug was added when cells reached 70% confluency. Cells were harvested by washing twice with PBS, lysing in lysis buffer (Nangia *et al.*, 2018) on ice, and spinning at 14,000 RPM at 4°C for 10 minutes to remove insoluble cell debris. Lysate protein concentrations were determined by a Bicinchoninic Acid assay (Thermo Fisher). Gel electrophoresis was performed using NuPage 4-12% Bis-Tris Midi gels (Invitrogen) in NuPage MOPS SDS Running Buffer (Invitrogen) followed by transfer onto PVDF membranes (Thermo Fisher). Following transfer, membranes blocked with 5% milk (Lab Scientific bioKEMIX) in Tris Buffered Saline with Tween 20 (TBS-T) and then incubated with primary antibody (1:1000, 1%BSA in TBS-T) at 4°C overnight. After washing in TBS-T), membranes were incubated with the appropriate secondary antibody (1:12500 in 2% skim milk in TBS-T) for 1 hour at room temperature. The following HRP-linked secondary antibodies were used: anti-rabbit IgG (CST7074) and anti-mouse IgG (CST7076). Membranes were removed from secondary antibodies and washed 3 times for 10 minutes each in TBS-T. Prior to imaging, membranes were incubated for 4 minutes SuperSignal West Femto Stable Peroxide & Luminol/Enhancer (Thermo Fisher) diluted 1:10 in 0.1 M tris-HCL pH 8.8 (Boston Bioproducts). Luminescence was imaged using a G:Box Chemi-XRQ system (Syngene). The following primary antibodies were used: pJNK T183/Y185 (CST4668), SAPK/JNK (CST9252), Bim (CST2933), pBCL-XL S62 (Invitrogen 44-428G), BCL-XL (CST2764), LKB1 (CST3050), pMCL-1 T163 (CST14765), pMCL-1 S159/T163 (CST4579), pMCL-1 S64 (CST13297), MCL-1 (BD Pharmingen 559027), pMKK4 S257/T261 (CST9156), MKK4 (CST9152), pMEK7 S271 (Thermo Fisher PA5-114604), pMEK7 T275 (Thermo Fisher PA5-114605), MKK7 (CST4172), DUSP10/MKP5 (CST3483), HA Tag (CST3724), β-Tubulin (CST2146), GAPDH (CST5174).

bioRxiv preprint doi: https://doi.org/10.1101/2022.09.29.510137; this version posted September 30, 2022. The copyright holder for this preprint (which was not certified by peer review) is the author/funder, who has granted bioRxiv a license to display the preprint in perpetuity. It is made available under aCC-BY-NC-ND 4.0 International license.

Protein Immunoprecipitation

Cells were seeded in either 10 cm or 15 cm plates and drug was added when cells reached 70% confluency. Cells were harvested after the treatment period and lysates were prepared using Tris Lysis Buffer with Protease Inhibitor Cocktail (Meso Scale Diagnostics) on ice. After normalization of total protein concentrations, Pierce Protein A/G Magnetic Beads (Thermo Fisher) and either mouse anti-human MCL-1 (BD Pharmingen 559027) or mouse anti-human BCL-XL (EMD Millipore MAB3121) antibodies were added to lysate aliquots and incubated at 4^{o}C overnight. A representative aliquot of the normalized whole cell lysate was saved for Western blot analysis. The immunoprecipitated fractions were separate using magnetic separation, washed three times with Tris Lysis Buffer on ice, proteins eluted by heating at 95^{o}C for 10 min with Tris Lysis Buffer and LDS Sample Buffer 4X (Invitrogen). For western blots, the rabbit anti-human MCL-1 (CST4572) antibody was used; all other antibodies were identical to those used for western blotting. For immunoprecipitation of HA-tagged BCL-XL, the Pierce Magnetic HA-Tag IP/Co-IP Kit (Thermo Fisher) was used following the manufacturer's protocol (specifically, the procedure for (A.) Manual IP/Co-IP and (B.) Elution Protocol 2 for reducing gel analysis).

siRNA-Mediated Gene Knockdown

siRNA transfection was performed using Lipofectamine RNAiMAX Transfection Reagent according to the manufacturer's protocol (Invitrogen, Cat# 13778075). In brief, cells were seeded in 6-well, 6 cm, or 10 cm plates and siRNA transfection was carried out when cells reached ~70% confluency. Prior to transfection, cells were placed in antibiotic-free media. 48 hours after transfection, cells were seeded for analysis of proliferation or immunoprecipitation or harvested for western blot. The following Invitrogen siRNA were used: NC (AM4611), MAPK8 (ID: s11152), MAPK9 (ID: s11159), NUAK1 (ID: s90), NUAK2 (ID: s37779), PRKAA1 (ID: s100), PRKAA2 (ID: s11056), PRKAB1 (ID: s11059), PRKAB2 (ID: s11062), SIK1 (ID: s45377), SIK2 (ID: s23355), SIK3 (ID: s23712), MARK1 (ID: s8511), MARK2 (ID: s4648), MARK3 (ID: s8514), MARK4 (ID: s33718), MAP2K4 (ID: s11182, s11183), MAP2K7 (ID: s11183, s11184), MCL-1 (ID: s8584, s8585), BCL2L1 (ID: s1920, s1921, s1922).

BH3 Profiling of Cell Lines

For each sample, 2x10^{6} cells were isolated, centrifuged at 500xg for 5 minutes, then the cell pellet was resuspended in 100µL PBS with 1µL Zombie Green viability dye (Biolegend, cat# 423111). Cells were stained at room temperature out of light for 15 minutes, then 400µL FACS Stain Buffer (2% FBS in PBS) was added to the sample to quench Zombie dye. Cells were then centrifuged at 500xg for 5 minutes then subjected to BH3 Profiling as previously described with indicated peptides and concentrations. After BH3 profiling, cells were permeabilized for intra-cellular staining with a saponin-based buffer (1% saponin, 10% BSA in PBS) and stained with an antibody for Cytochrome C AlexaFluor 647 (Biolegend, 612310) used at 1:2000 dilution and DAPI. Cells were left to stain overnight at 4°C and analyzed by flow cytometry (Attune NxT) the following day.

BH3 Profiling of Primary Patient Samples

Surgical resections were minced by scalpels to ~1mm^{3}. Minced explants were cultured in RPMI1640 + 10% FBS overnight in the absence or presence of drugs. Immediately prior to BH3 profiling, tissue was further dissociated by collagenase/dispase enzymatic dissociation for 30 minutes at 37°C. Samples were then strained through 100µM filter to isolate single cells. For each sample, 2x10^{6} cells were isolated, centrifuged at 500xg for 5 minutes, then the cell pellet was resuspended in 100µL PBS with 1µL Zombie Green viability dye (Biolegend, cat# 423111). Cells were stained at room temperature out of light for 15 minutes, then 400µL FACS Stain Buffer (2% FBS in PBS) was added to the sample to quench Zombie dye. Cells were then centrifuged at

bioRxiv preprint doi: https://doi.org/10.1101/2022.09.29.510137; this version posted September 30, 2022. The copyright holder for this preprint (which was not certified by peer review) is the author/funder, who has granted bioRxiv a license to display the preprint in perpetuity. It is made available under aCC-BY-NC-ND 4.0 International license.

500xg for 5 minutes, then resuspended in 100µL FACS Stain Buffer. Cells were then stained with the following conjugated cell-surface marker antibodies at 1:50 dilutions: CD326 (EpCAM) PE (Biolegend, 324206) and CD45 BV786 (Biolegend, 304048). Cells were then centrifuged at 500xg for 5 minutes and subjected to BH3 Profiling as previously described with indicated peptides and concentrations. After BH3 profiling, cells were permeabilized for intra-cellular staining with a saponin-based buffer (1% saponin, 10% BSA in PBS) and stained with an antibody for Cytochrome C AlexaFluor 647 (Biolegend, 612310) used at 1:2000 dilution and DAPI. Cells were left to stain overnight at 4°C and analyzed by flow cytometry (Attune NxT) the following day. Cells of interest were identified by positive DAPI, negative Zombie, negative CD45, and positive EpCAM staining.

Phosphoproteomic Analysis

Frozen cell pellets were lysed, obtained proteins reduced with DTT and alkylated with iodoacetamide, precipitated following the MeOH/CHCl3 protocol, and digested with LysC and trypsin, followed by phophopeptide enrichment as previously described (PMID: 31606085). For each sample 2.5 mg of peptides were subjected to phosphopeptide enrichment on TiO2 beads (GL Sciences, Japan). Phosphopeptides were labeled with TMT10plex reagents (Thermo Fisher Scientific), pooled, and were fractionated into 24 fractions using basic pH reversed phase chromatography essentially as described previously (PMID: 26700037). Those were dried, re-suspended in 5% ACN/5% formic acid, and analyzed in 3-hour runs via LC-M2/MS3 on an Orbitrap FusionLumos mass spectrometer using the Simultaneous Precursor Selection (SPS) supported MS3 method (PMID: 24927332; PMID: 21963607) essentially as described previously (PMID: 25521595). Two MS2 spectra were acquired for each peptide using CID and HCD fragmentation as described earlier (PMID: 29487189) and the gained MS2 spectra were assigned using a SEQUEST-based in-house built proteomics analysis platform (PMID: 21183079) allowing phosphorylation of serine, threonine, and tyrosine residues as a variable modification. The Ascore algorithm was used to evaluate the correct assignment of phosphorylation within the peptide sequence (PMID: 16964243). Based on the target-decoy database search strategy (PMID: 17327847) and employing linear discriminant analysis and posterior error histogram sorting, peptide and protein assignments were filtered to false discovery rate (FDR) of < 1% (PMID: 21183079). Peptides with sequences that were contained in more than one protein sequence from the UniProt database (2014) were assigned to the protein with most matching peptides (PMID: 21183079). Only MS3 with an average signal-to-noise value of larger than 40 per reporter ion as well as with an isolation specificity (PMID: 21963607) of larger than 0.75 were considered for quantification. A two-step normalization of the protein TMT-intensities was performed by first normalizing the protein intensities over all acquired TMT channels for each protein based on the median average protein intensity calculated for all proteins. To correct for slight mixing errors of the peptide mixture from each sample a median of the normalized intensities was calculated from all protein intensities in each TMT channel and the protein intensities were normalized to the median value of these median intensities.

Proteomic Analysis

50 µg of the of the resulting peptides after tryptic digest as described above were subsequently labeled using TMT-10plex reagents (Thermo Scientific) according to manufacturer's instructions. Labeled samples got combined and fractionated using a basic reversed phase hplc (PMID: 26700037). The resulting fractions were analyzed in an 3h reversed phase LC-MS2/MS3 run on an Orbitrap FusionLumos. MS3 isolation for quantification used Simultaneous Precursor Selection (SPS) as previously described (PMID: 21963607, PMID: 24927332, PMID: 25521595). Proteins were identified based on MS2 spectra using the sequest algorithm searching against a human data base (uniprot 2014) (PMID: 24226387) using an in house-built platform (PMID: 21183079). Search strategy included a target-decoy database-based search in order to filter

bioRxiv preprint doi: https://doi.org/10.1101/2022.09.29.510137; this version posted September 30, 2022. The copyright holder for this preprint (which was not certified by peer review) is the author/funder, who has granted bioRxiv a license to display the preprint in perpetuity. It is made available under aCC-BY-NC-ND 4.0 International license.

against a false-discovery rate (FDR) of protein identifications of less than 1% (PMID: 17327847). For quantification only MS3 with an average signal-to-noise value of larger than 40 per reporter ion as well as with an isolation specificity (PMID: 21963607) of larger than 0.75 were considered and a two-step normalization as described above was performed.

Phospho-proteomic Signature Analysis

Phospho-signature analysis was performed using PTM-Signature Enrichment Analysis (PMT-SEA), a modified version of ssGSEA2.0 (https://github.com/broadinstitute/ssGSEA2.0). Briefly, relative log-fold increases/decreases were calculated by comparing the levels of phospho-peptides in each group. Relative log-fold increases/decreases were imported into the PMT-SEA package and compared against the PTM signatures database (PTMsigDB). Significant signatures were exported, ranked and compared between groups (for example LKB1-positive versus LKB1-negative isogenic pair).

bioRxiv preprint doi: https://doi.org/10.1101/2022.09.29.510137; this version posted September 30, 2022. The copyright holder for this preprint (which was not certified by peer review) is the author/funder, who has granted bioRxiv a license to display the preprint in perpetuity. It is made available under aCC-BY-NC-ND 4.0 International license.

ACKNOWLEDGEMENTS

We thank the patients and their families who provided tumor tissue for analysis and generation of patient-derived models. We thank members of the Hata lab and MGH Thoracic Oncology Group for helpful discussion and support. We thank Dr. Kwok-Kin Wong for providing the pBABE-EV and pBABE-LKB1 plasmids. This study was funded by support from the NIH F32 CA250231 (C.L.), Mark Foundation for Cancer Research (The EXTOL Project) (A.N.H.), Stand Up To Cancer–American Cancer Society Lung Cancer Dream Team Translational Research Grant (SU2C-AACR-DT17-15) (A.N.H.), the Ludwig Center at Harvard (A.N.H.), a research grant provided by Amgen, Inc. (A.N.H.), and by Be a Piece of the Solution Research Fund at MGH. Stand Up To Cancer (SU2C) is a division of the Entertainment Industry Foundation. Research grants are administered by the American Association for Cancer Research, the Scientific Partner of SU2C.

AUTHOR CONTRIBUTIONS

C.L, M.U.S., Y.S., C.F., J.O., J.K., S.E..C, A.O., M.W. performed the experiments. R.H., J.L. contributed human samples and/or data. S.E.C., A.O., M.W. developed patient-derived cell lines and PDX models. C.L.**,** R.M. and A.N.H. performed data analysis and interpretation. S.C., A.Y.S., K.R., J.R.L., P.E.H. provided KRAS and MCL-1 inhibitors used in this study. C.L., J.O., C.N., K.S., W.H., P.E.H., A.N.H. were involved with study design. C.L. and A.N.H. wrote the manuscript. All authors discussed the results and commented on the manuscript.

COMPETING INTERESTS STATEMENT

A.N.H. has received research support from Amgen, Eli Lilly, Pfizer, BridgeBio, Nuvalent Inc., Roche/Genentech, Blueprint Medicines, Scorpion Therapeutics, Bristol-Myers Squibb, C4 Therapeutics, Novartis and Relay Therapeutics; has served as a compensated consultant for Nuvalent, Tolremo Therapeutics, Engine Biosciences and TigaTx. RSH has served as a compensated consultant for Abbvie, Daichii Sankyo, EMD Serono, Novartis, Regeneron. Research funding to institution, not to self: Abbvie, Agios, Corvus, Exelixis, Genentech, Lilly, Mirati, Novartis, Turning Point. J.J.L. reports consulting fees from Genentech, C4 Therapeutics, Blueprint Medicines, Nuvalent, Bayer, Elevation Oncology, Novartis, Mirati Therapeutics, and Turning Point Therapeutics; honorarium and travel support from Pfizer; institutional research funding from Hengrui Therapeutics, Turning Point Therapeutics, Neon Therapeutics, Relay Therapeutics, Bayer, Elevation Oncology, Roche, Linnaeus Therapeutics, Nuvalent, and Novartis; and CME funding from OncLive, MedStar Health, and Northwell Health. C.S.N. owns equity (stock) in Opko Therapeutics and has received royalty income from ThermoFisher (previously Life Sciences). S.C., A.Y.S., K.R., J.R.L., P.E.H are employees of and have ownership (including stock, patents, etc.) interest in Amgen. The remaining authors declare no competing interests.

bioRxiv preprint doi: https://doi.org/10.1101/2022.09.29.510137; this version posted September 30, 2022. The copyright holder for this preprint (which was not certified by peer review) is the author/funder, who has granted bioRxiv a license to display the preprint in perpetuity. It is made available under aCC-BY-NC-ND 4.0 International license.

FIGURE LEGENDS

Figure 1. LKB1 loss confers sensitivity to combined MAPK + MCL-1 inhibition in *KRAS*-mutant NSCLC models. A. *KRAS*-mutant NSCLC cell lines H23 and H358 were treated with increasing doses of sotorasib alone or in combination with a fixed dose of 1 µM of AMG 176 for three days. Relative cell number was assessed by CellTiter-Glo (CTG) viability assay. B. Relative increased efficacy of sotorasib + AMG 176 combination compared to sotorasib alone (ΔAUC – see Fig. S2A for explanation) against $KRAS^{G12C}$ NSCLC cell lines. C. Relative increase in efficacy of trametinib + AMG 176 compared to trametinib alone. D. Comparison of ΔAUC between *KRAS*-mutant NSCLC cell lines stratified according to LKB1 status (Student t test). E. *KRAS*-mutant NSCLC cell lines were treated with 0.1 µM of trametinib, 1 µM of AMG 176 or 0.1 µM of trametinib + 1 µM of AMG 176 for 72 hours and apoptosis was assessed by PI-annexin staining and flow cytometry. F. Cell viability of isogenic (LKB1-deficient H2030, expressing empty vector or LKB1; LKB1 wild-type H358 with CRISPR knock-out of LKB1 or GFP control) $KRAS^{G12C}$-mutant NSCLC cell lines after treatment with sotorasib alone or in combination with 1 µM of AMG 176. G-H. Comparison of relative ΔAUC for isogenic LKB1-proficient and deficient *KRAS*-mutant cell line pairs. Re-expression of LKB1 decreased MCL-1 sensitivity of LKB1-deficient cells, whereas deletion of LKB1 sensitized LKB1 wild-type cells. I. Apoptotic response of isogenic *KRAS*-mutant NSCLC cell lines after treatment with trametinib + 1 µM of AMG 176. Re-expression of LKB1 decreased apoptosis of LKB1-deficient cells, whereas deletion of LKB1 increased apoptosis of LKB1 wild-type cells. J. Subcutaneous xenograft tumors were established from H2030 EV and H2030 LKB1 cell lines and mice were treated with vehicle, sotorasib (30mg/kg), trametinib (3 mg/kg), or in combination with AMG 176 (50mg/kg). Re-expression of LKB1 decreased sensitivity to MCL-1 combination. Data shown are mean and S.E.M of 3-6 mice per arm, statistical difference between single agent and combination arms was determined using mixed effects model (*p<0.05, **p<0.01).

Figure 2. JNK activation in LKB1-deficient cells underlies sensitivity to MCL-1 inhibition. A. Phosphoproteomic analysis of isogenic *KRAS*-mutant NSCLC cell lines treated with 0.1 µM of trametinib for 48 hours. B. Differential enrichment of phosphopeptide signatures in trametinib-treated isogenic cell line pairs. Phosphopeptide signatures and normalized enrichment scores (NES) were calculated using ssGSEA2.0/PTM-SEA. Dashed line indicates adjusted p value = 0.05. C. Western blot analysis of isogenic *KRAS*-mutant NSCLC cell lines after treatment with 1 µM sotorasib + 1 µM AMG 176 (SA) or 0.1 µM trametinib + 1 µM AMG 176 (TA) for 8 hours. SA: sotorasib + AMG 176. D. Densitometry quantification of western blots of isogenic cell lines after treatment with SA or TA. Individual biological replicates are shown, error bars represent S.E.M. (**p<0.01, ***p<0.001, ratio-paired t test). E. Fold induction of phospho-JNK in LKB1-deficient or wild-type *KRAS*-mutant NSCLC cell lines after treatment with 0.1 µM trametinib + 1 µM AMG 176 for 8 hours. Data shown are quantification of densitometry levels from western blots of phospho-JNK normalized to total JNK, in drug-treated compared to vehicle cells. F. Change in cell number of H2030 EV cells with siRNA knockdown of JNK1+2 or negative control (siNC) after treatment with 0.1 µM trametinib or 1 µM sotorasib in combination with 1 µM AMG 176 quantified by Incucyte imaging. G. Change in viability (ΔAUC) of H2030 EV cell-line with knockdown of JNK1+2 or negative control (siNC) after treatment with trametinib or sotorasib alone or in combination with AMG 176.

Figure 3. Suppression of JNK activation by LKB1 is mediated by NUAK kinases. A. Schematic of approach using siRNA knockdown to determine which LKB1 substrate mediates the effect of LKB1 on MCL-1 dependency. B. Knockdown of NUAK1/2 restores sensitivity (ΔAUC) to combined sotorasib or trametinib + AMG 176. H2030 EV cells or H2030 LBK1 cells transfected with corresponding siRNAs were treated with sotorasib or trametinib in the absence or presence

bioRxiv preprint doi: https://doi.org/10.1101/2022.09.29.510137; this version posted September 30, 2022. The copyright holder for this preprint (which was not certified by peer review) is the author/funder, who has granted bioRxiv a license to display the preprint in perpetuity. It is made available under aCC-BY-NC-ND 4.0 International license.

of AMG 176 (1 μM) and viability was determined after 3 days. C. Cell viability H2030 EV or H2030 LKB1 cells transfected with siNUAK1+2 or siNC after treatment with vehicle, 1 μM sotorasib, 0.1 μM trametinib, 1 μM AMG 176, or combination for 3 days. Data are mean and S.E.M. for triplicate biological replicates (****p < 0.0001, unpaired t test). D. NUAK1/2 knockdown restores phospho-JNK induction after trametinib or trametinib + AMG 176 in H2030 LKB1 cells to the level of H2030 control cells. Cells were transfected with the indicated siRNAs and then treated with trametinib (0.1 μM) for 48 hours or trametinib for 48 hours followed by AMG 176 for 4 hours.

Figure 4. LKB1 loss increases BIM:MCL-1 interaction and creates an MCL-1 dependent state. A. Schematic of BH3 profiling experimental setup. The change in priming (Δ Priming) is measured before and after treatment with trametinib (0.1 μM) as depicted in Fig. S6B. B. Change in dependence (cytochrome c release in response to 10 μM MS-1 peptide) induced by trametinib in isogenic *KRAS*-mutant NSCLC cell lines. C. Co-immunoprecipitation (Co-IP) assessment of H2030 cells after treatment with 0.1 μM trametinib for 24 hours. D. Quantification of BIM bound to MCL-1 versus BCL-XL in *KRAS*-mutant NSCLC cells after treatment with trametinib. BIM:MCL-1 and BIM:BCL-XL binding ratios were calculated from densitometry measurements as described in Fig. S7A. Input and IP protein bands were quantified from the same blot. E. Co-IP assessment of BIM bound to MCL-1 in H2030 EV and H2030 LKB1 cells after treatment with vehicle, trametinib (0.1) for 24 hours or trametinib for 24h followed by AMG 176 (1 μM) for 4 hours. F. BIM:MCL-1 binding ratios after 24 hours trametinib treatment (left) or vehicle (right) in isogenic cell lines. Binding ratios were calculated from densitometry measurements as shown in Fig. S7C.

Figure 5. JNK phosphorylates BCL-XL to drive an MCL-1 dependent state. A. Time course of BCL-XL phosphorylation (S62) in isogenic H2030 and H358 cells by western blot after treatment with 0.1 μM trametinib + 1 μM AMG 176. B. JNK1/2 knockdown in H2030 EV cells decreases drug-induced BCL-XL phosphorylation to a similar level as in H2030 LKB1 cells. After siRNA transfection, cells were treated with 0.1 μM trametinib for 48h or trametinib for 48h followed by 1 μM AMG 176 for 4 hours. C. Experimental approach for expressing MCL-1 & BCL-XL phospho-site mutants while suppressing endogenous MCL-1 and BCL-XL. Interrogated phosphorylation sites are designated in yellow, phosphomimetic sites in red. D. MCL-1 phospho-site mutants do not reduced sensitivity to MCL-1 inhibition (ΔAUC). After induction of mutant MCL-1 (or WT control) and knockdown of endogenous MCL-1, H2030 EV cells were treated with trametinib in the absence or presence of AMG 176 (1 μM) and viability was determined after 3 days. **E-F.** BCL-XL S62A mutant decreases MCL-1 sensitivity. After induction of BCL-XL S62A (or WT control) and knockdown of endogenous BCL-XL, H2030 EV cells were treated with sotorasib or trametinib alone or in the presence of AMG 176 (1 μM) and viability was determined after 3 days. **G-H.** H2030 EV cells expressing inducible WT or S62A mutant BCL-XL S62A (G) or H2030 LKB1 cells expressing inducible WT or BCL-XL S62E phosphomimetic were treated with 0.1 μM trametinib or 0.1 μM sotorasib in combination with 1 μM AMG 176 (TA or SA, respectively) and cell number was quantified by Incucyte imaging.

Figure 6. JNK activation drives an MCL-1 dependent state by modulating BIM:BCL-XL interactions. A. Schematic of experimental approach to investigating BIM sequestration upon displacement from MCL-1. B. Co-IP assessment of BIM bound to MCL-1 and BCL-XL in H2030 (LKB1-deficient) and SW1573 (LKB1 wild-type) cells after treatment with 0.1 μM trametinib for 24 hours followed by 1 μM AMG 176 for 4 hours. C. Co-IP assessment of BIM bound to BCL-XL and MCL-1 in H2030 EV and LKB1 cells after treatment with 0.1 μM trametinib for 24 hours followed by 1 μM AMG 176 for 4 hours. D. Co-IP assessment of BIM bound to BCL-XL and MCL-1 in H2030 EV with JNK knockdown after treatment with 0.1 μM trametinib for 24 hours + 1 μM AMG 176 for 4 hours. E. Co-IP assessment of BIM bound to WT BCL-XL and BCL-XL mutants in H2030 EV (S62A) and H2030 LKB1 (S62E) cells after treatment with 0.1 μM trametinib for 24 hours

bioRxiv preprint doi: https://doi.org/10.1101/2022.09.29.510137; this version posted September 30, 2022. The copyright holder for this preprint (which was not certified by peer review) is the author/funder, who has granted bioRxiv a license to display the preprint in perpetuity. It is made available under aCC-BY-NC-ND 4.0 International license.

followed 1 μM AMG 176 for 4 hours. HA-tag pull downs are specific for inducible constructs. F. Effect of NUAK1/2 knockdown on BCL-XL S62 phosphorylation in response to treatment with 0.1 μM trametinib for 48h (T) or trametinib for 48 hours followed by 1 μM AMG 176 (TA) for 4 hours. G. Model depicting how LKB1 loss leads to an MCL-1-dependent state and sensitizes *KRAS*-mutant NSCLCs to combined KRAS or MEK + MCL-1 inhibition.

Figure 7. LKB1 loss predicts sensitivity to KRAS^{G12C} + MCL-1 inhibition in *KRAS*^{G12C}-mutant NSCLC PDX tumors and patient tumor explants. A. *KRAS*^{G12C}-mutant NSCLC tumor cells were collected for BH3 profiling and assessment of BIM:MCL-1 interactions after ex vivo treatment with sotorasib or trametinib. B. Change in total (PUMA 10 peptide), MCL-1 (MS1 10 peptide) and BCL-XL (HRK 100 peptide) dependent priming of tumor cells after ex vivo treatment with 0.1 μM trametinib or 1 μM sotorasib treatment. C. Co-IP assessment of BIM:MCL-1 interaction in tumor cells isolated from pleural fluid after *ex vivo* treatment with 0.1 μM trametinib (T) or 1 μM sotorasib (S) for 16 hours. D. Mice bearing *KRAS*^{G12C}-mutant NSCLC patient derived xenograft (PDX) tumors were treated with sotorasib (100 mg/kg) for 3 days and harvested for BH3 profiling. Data shown is the difference in MCL-1 dependent priming (MS1 peptide) between vehicle and sotorasib treated tumors. E. Mice bearing *KRAS*^{G12C}-mutant NSCLC PDX tumors (LKB1-deficient - MGH1112-1, MGH1138-1, MGH1196-2; LKB1 wild-type - MGH1145-1) were treated with vehicle, sotorasib (100 mg/kg) or sotorasib (100 mg/kg) + AMG 176 (50 mg/kg). Data shown are mean and S.E.M. of N=3-7 animals per arm (**p<0.01, ***p<0.001 as determined by mixed-effects model).

bioRxiv preprint doi: https://doi.org/10.1101/2022.09.29.510137; this version posted September 30, 2022. The copyright holder for this preprint (which was not certified by peer review) is the author/funder, who has granted bioRxiv a license to display the preprint in perpetuity. It is made available under aCC-BY-NC-ND 4.0 International license.

REFERENCES

Amin, N., Khan, A., St Johnston, D., Tomlinson, I., Martin, S., Brenman, J., and McNeill, H. (2009). LKB1 regulates polarity remodeling and adherens junction formation in the Drosophila eye. Proc Natl Acad Sci U S A *106*, 8941-8946. 10.1073/pnas.0812469106.

Baas, A.F., Kuipers, J., van der Wel, N.N., Batlle, E., Koerten, H.K., Peters, P.J., and Clevers, H.C. (2004). Complete polarization of single intestinal epithelial cells upon activation of LKB1 by STRAD. Cell *116*, 457-466. 10.1016/s0092-8674(04)00114-x.

Banerjee, S., Zagorska, A., Deak, M., Campbell, D.G., Prescott, A.R., and Alessi, D.R. (2014). Interplay between Polo kinase, LKB1-activated NUAK1 kinase, PP1betaMYPT1 phosphatase complex and the SCFbetaTrCP E3 ubiquitin ligase. Biochem J *461*, 233-245. 10.1042/BJ20140408.

Barnes, A.P., Lilley, B.N., Pan, Y.A., Plummer, L.J., Powell, A.W., Raines, A.N., Sanes, J.R., and Polleux, F. (2007). LKB1 and SAD kinases define a pathway required for the polarization of cortical neurons. Cell *129*, 549-563. 10.1016/j.cell.2007.03.025.

Becker, E.B., Howell, J., Kodama, Y., Barker, P.A., and Bonni, A. (2004). Characterization of the c-Jun N-terminal kinase-BimEL signaling pathway in neuronal apoptosis. J Neurosci *24*, 8762-8770. 10.1523/JNEUROSCI.2953-04.2004.

Blazejewski, S.M., Bennison, S.A., Liu, X., and Toyo-Oka, K. (2021). High-throughput kinase inhibitor screening reveals roles for Aurora and Nuak kinases in neurite initiation and dendritic branching. Sci Rep *11*, 8156. 10.1038/s41598-021-87521-3.

Caenepeel, S., Brown, S.P., Belmontes, B., Moody, G., Keegan, K.S., Chui, D., Whittington, D.A., Huang, X., Poppe, L., Cheng, A.C., et al. (2018). AMG 176, a Selective MCL1 Inhibitor, Is Effective in Hematologic Cancer Models Alone and in Combination with Established Therapies. Cancer Discov. 10.1158/2159-8290.CD-18-0387.

Cancer Genome Atlas Research, N. (2014). Comprehensive molecular profiling of lung adenocarcinoma. Nature *511*, 543-550. 10.1038/nature13385.

Canon, J., Rex, K., Saiki, A.Y., Mohr, C., Cooke, K., Bagal, D., Gaida, K., Holt, T., Knutson, C.G., Koppada, N., et al. (2019). The clinical KRAS(G12C) inhibitor AMG 510 drives anti-tumour immunity. Nature *575*, 217-223. 10.1038/s41586-019-1694-1.

Chen, Z., Cheng, K., Walton, Z., Wang, Y., Ebi, H., Shimamura, T., Liu, Y., Tupper, T., Ouyang, J., Li, J., et al. (2012). A murine lung cancer co-clinical trial identifies genetic modifiers of therapeutic response. Nature *483*, 613-617. 10.1038/nature10937.

Corazza, N., Jakob, S., Schaer, C., Frese, S., Keogh, A., Stroka, D., Kassahn, D., Torgler, R., Mueller, C., Schneider, P., and Brunner, T. (2006). TRAIL receptor-mediated JNK activation and Bim phosphorylation critically regulate Fas-mediated liver damage and lethality. J Clin Invest *116*, 2493-2499. 10.1172/JCI27726.

Corcoran, R.B., Cheng, K.A., Hata, A.N., Faber, A.C., Ebi, H., Coffee, E.M., Greninger, P., Brown, R.D., Godfrey, J.T., Cohoon, T.J., et al. (2013). Synthetic lethal interaction of combined BCL-XL and MEK inhibition promotes tumor regressions in KRAS mutant cancer models. Cancer Cell *23*, 121-128. 10.1016/j.ccr.2012.11.007.

Cracan, V., Titov, D.V., Shen, H., Grabarek, Z., and Mootha, V.K. (2017). A genetically encoded tool for manipulation of NADP(+)/NADPH in living cells. Nat Chem Biol *13*, 1088-1095. 10.1038/nchembio.2454.

Cragg, M.S., Harris, C., Strasser, A., and Scott, C.L. (2009). Unleashing the power of inhibitors of oncogenic kinases through BH3 mimetics. Nat Rev Cancer *9*, 321-326. 10.1038/nrc2615.

Cragg, M.S., Jansen, E.S., Cook, M., Harris, C., Strasser, A., and Scott, C.L. (2008). Treatment of B-RAF mutant human tumor cells with a MEK inhibitor requires Bim and is enhanced by a BH3 mimetic. J Clin Invest *118*, 3651-3659. 10.1172/JCI35437.

bioRxiv preprint doi: https://doi.org/10.1101/2022.09.29.510137; this version posted September 30, 2022. The copyright holder for this preprint (which was not certified by peer review) is the author/funder, who has granted bioRxiv a license to display the preprint in perpetuity. It is made available under aCC-BY-NC-ND 4.0 International license.

Derijard, B., Hibi, M., Wu, I.H., Barrett, T., Su, B., Deng, T., Karin, M., and Davis, R.J. (1994). JNK1: a protein kinase stimulated by UV light and Ha-Ras that binds and phosphorylates the c-Jun activation domain. Cell *76*, 1025-1037. 10.1016/0092-8674(94)90380-8.

Domina, A.M., Vrana, J.A., Gregory, M.A., Hann, S.R., and Craig, R.W. (2004). MCL1 is phosphorylated in the PEST region and stabilized upon ERK activation in viable cells, and at additional sites with cytotoxic okadaic acid or taxol. Oncogene *23*, 5301-5315. 10.1038/sj.onc.1207692.

Egan, D.F., Shackelford, D.B., Mihaylova, M.M., Gelino, S., Kohnz, R.A., Mair, W., Vasquez, D.S., Joshi, A., Gwinn, D.M., Taylor, R., et al. (2011). Phosphorylation of ULK1 (hATG1) by AMP-activated protein kinase connects energy sensing to mitophagy. Science *331*, 456-461. 10.1126/science.1196371.

El Fajoui, Z., Toscano, F., Jacquemin, G., Abello, J., Scoazec, J.Y., Micheau, O., and Saurin, J.C. (2011). Oxaliplatin sensitizes human colon cancer cells to TRAIL through JNK-dependent phosphorylation of Bcl-xL. Gastroenterology *141*, 663-673. 10.1053/j.gastro.2011.04.055.

Faber, A.C., Coffee, E.M., Costa, C., Dastur, A., Ebi, H., Hata, A.N., Yeo, A.T., Edelman, E.J., Song, Y., Tam, A.T., et al. (2014). mTOR inhibition specifically sensitizes colorectal cancers with KRAS or BRAF mutations to BCL-2/BCL-XL inhibition by suppressing MCL-1. Cancer Discov *4*, 42-52. 10.1158/2159-8290.CD-13-0315.

Follis, A.V., Llambi, F., Kalkavan, H., Yao, Y., Phillips, A.H., Park, C.G., Marassi, F.M., Green, D.R., and Kriwacki, R.W. (2018). Regulation of apoptosis by an intrinsically disordered region of Bcl-xL. Nat Chem Biol *14*, 458-465. 10.1038/s41589-018-0011-x.

Fraser, C., Ryan, J., and Sarosiek, K. (2019). BH3 Profiling: A Functional Assay to Measure Apoptotic Priming and Dependencies. Methods Mol Biol *1877*, 61-76. 10.1007/978-1-4939-8861-7_4.

Galan-Cobo, A., Sitthideatphaiboon, P., Qu, X., Poteete, A., Pisegna, M.A., Tong, P., Chen, P.H., Boroughs, L.K., Rodriguez, M.L.M., Zhang, W., et al. (2019). LKB1 and KEAP1/NRF2 Pathways Cooperatively Promote Metabolic Reprogramming with Enhanced Glutamine Dependence in KRAS-Mutant Lung Adenocarcinoma. Cancer Res *79*, 3251-3267. 10.1158/0008-5472.CAN-18-3527.

Gan, B., Hu, J., Jiang, S., Liu, Y., Sahin, E., Zhuang, L., Fletcher-Sananikone, E., Colla, S., Wang, Y.A., Chin, L., and Depinho, R.A. (2010). Lkb1 regulates quiescence and metabolic homeostasis of haematopoietic stem cells. Nature *468*, 701-704. 10.1038/nature09595.

Hallin, J., Engstrom, L.D., Hargis, L., Calinisan, A., Aranda, R., Briere, D.M., Sudhakar, N., Bowcut, V., Baer, B.R., Ballard, J.A., et al. (2020). The KRASG12C Inhibitor MRTX849 Provides Insight toward Therapeutic Susceptibility of KRAS-Mutant Cancers in Mouse Models and Patients. Cancer Discovery *10*, 54-71. 10.1158/2159-8290.cd-19-1167.

Hata, A.N., Engelman, J.A., and Faber, A.C. (2015). The BCL2 Family: Key Mediators of the Apoptotic Response to Targeted Anticancer Therapeutics. Cancer Discov *5*, 475-487. 10.1158/2159-8290.CD-15-0011.

Hata, A.N., Yeo, A., Faber, A.C., Lifshits, E., Chen, Z., Cheng, K.A., Walton, Z., Sarosiek, K.A., Letai, A., Heist, R.S., et al. (2014). Failure to induce apoptosis via BCL-2 family proteins underlies lack of efficacy of combined MEK and PI3K inhibitors for KRAS-mutant lung cancers. Cancer Res *74*, 3146-3156. 10.1158/0008-5472.CAN-13-3728.

Hayes, J.D., Dinkova-Kostova, A.T., and Tew, K.D. (2020). Oxidative Stress in Cancer. Cancer Cell *38*, 167-197. 10.1016/j.ccell.2020.06.001.

Hibi, M., Lin, A., Smeal, T., Minden, A., and Karin, M. (1993). Identification of an oncoprotein- and UV-responsive protein kinase that binds and potentiates the c-Jun activation domain. Genes Dev *7*, 2135-2148. 10.1101/gad.7.11.2135.

Hollstein, P.E., Eichner, L.J., Brun, S.N., Kamireddy, A., Svensson, R.U., Vera, L.I., Ross, D.S., Rymoff, T.J., Hutchins, A., Galvez, H.M., et al. (2019). The AMPK-Related Kinases SIK1 and SIK3 Mediate Key Tumor-Suppressive Effects of LKB1 in NSCLC. Cancer Discov *9*, 1606-1627. 10.1158/2159-8290.CD-18-1261.

bioRxiv preprint doi: https://doi.org/10.1101/2022.09.29.510137; this version posted September 30, 2022. The copyright holder for this preprint (which was not certified by peer review) is the author/funder, who has granted bioRxiv a license to display the preprint in perpetuity. It is made available under aCC-BY-NC-ND 4.0 International license.

910 Hubner, A., Barrett, T., Flavell, R.A., and Davis, R.J. (2008). Multisite phosphorylation regulates Bim
911 stability and apoptotic activity. Mol Cell *30*, 415-425. 10.1016/j.molcel.2008.03.025.
912 Inoki, K., Zhu, T., and Guan, K.L. (2003). TSC2 mediates cellular energy response to control cell growth
913 and survival. Cell *115*, 577-590. 10.1016/s0092-8674(03)00929-2.
914 Inoshita, S., Takeda, K., Hatai, T., Terada, Y., Sano, M., Hata, J., Umezawa, A., and Ichijo, H. (2002).
915 Phosphorylation and inactivation of myeloid cell leukemia 1 by JNK in response to oxidative stress. J Biol
916 Chem *277*, 43730-43734. 10.1074/jbc.M207951200.
917 Janes, M.R., Zhang, J., Li, L.S., Hansen, R., Peters, U., Guo, X., Chen, Y., Babbar, A., Firdaus, S.J., Darjania,
918 L., et al. (2018). Targeting KRAS Mutant Cancers with a Covalent G12C-Specific Inhibitor. Cell *172*, 578-
919 589 e517. 10.1016/j.cell.2018.01.006.
920 Janne, P.A., Riely, G.J., Gadgeel, S.M., Heist, R.S., Ou, S.I., Pacheco, J.M., Johnson, M.L., Sabari, J.K.,
921 Leventakos, K., Yau, E., et al. (2022). Adagrasib in Non-Small-Cell Lung Cancer Harboring a KRAS(G12C)
922 Mutation. N Engl J Med *387*, 120-131. 10.1056/NEJMoa2204619.
923 Jeon, S.M., Chandel, N.S., and Hay, N. (2012). AMPK regulates NADPH homeostasis to promote tumour
924 cell survival during energy stress. Nature *485*, 661-665. 10.1038/nature11066.
925 Ji, H., Ramsey, M.R., Hayes, D.N., Fan, C., McNamara, K., Kozlowski, P., Torrice, C., Wu, M.C., Shimamura,
926 T., Perera, S.A., et al. (2007). LKB1 modulates lung cancer differentiation and metastasis. Nature *448*,
927 807-810. 10.1038/nature06030.
928 Jordan, E.J., Kim, H.R., Arcila, M.E., Barron, D., Chakravarty, D., Gao, J., Chang, M.T., Ni, A., Kundra, R.,
929 Jonsson, P., et al. (2017). Prospective Comprehensive Molecular Characterization of Lung
930 Adenocarcinomas for Efficient Patient Matching to Approved and Emerging Therapies. Cancer Discov *7*,
931 596-609. 10.1158/2159-8290.CD-16-1337.
932 Kandoth, C., McLellan, M.D., Vandin, F., Ye, K., Niu, B., Lu, C., Xie, M., Zhang, Q., McMichael, J.F.,
933 Wyczalkowski, M.A., et al. (2013). Mutational landscape and significance across 12 major cancer types.
934 Nature *502*, 333-339. 10.1038/nature12634.
935 Kharbanda, S., Saxena, S., Yoshida, K., Pandey, P., Kaneki, M., Wang, Q., Cheng, K., Chen, Y.N., Campbell,
936 A., Sudha, T., et al. (2000). Translocation of SAPK/JNK to mitochondria and interaction with Bcl-x(L) in
937 response to DNA damage. J Biol Chem *275*, 322-327. 10.1074/jbc.275.1.322.
938 Kotschy, A., Szlavik, Z., Murray, J., Davidson, J., Maragno, A.L., Le Toumelin-Braizat, G., Chanrion, M.,
939 Kelly, G.L., Gong, J.N., Moujalled, D.M., et al. (2016). The MCL1 inhibitor S63845 is tolerable and
940 effective in diverse cancer models. Nature *538*, 477-482. 10.1038/nature19830.
941 Krug, K., Mertins, P., Zhang, B., Hornbeck, P., Raju, R., Ahmad, R., Szucs, M., Mundt, F., Forestier, D.,
942 Jane-Valbuena, J., et al. (2019). A Curated Resource for Phosphosite-specific Signature Analysis. Mol Cell
943 Proteomics *18*, 576-593. 10.1074/mcp.TIR118.000943.
944 Kullmann, L., and Krahn, M.P. (2018). Controlling the master-upstream regulation of the tumor
945 suppressor LKB1. Oncogene *37*, 3045-3057. 10.1038/s41388-018-0145-z.
946 Lei, K., and Davis, R.J. (2003). JNK phosphorylation of Bim-related members of the Bcl2 family induces
947 Bax-dependent apoptosis. Proc Natl Acad Sci U S A *100*, 2432-2437. 10.1073/pnas.0438011100.
948 Li, F., Han, X., Li, F., Wang, R., Wang, H., Gao, Y., Wang, X., Fang, Z., Zhang, W., Yao, S., et al. (2015). LKB1
949 Inactivation Elicits a Redox Imbalance to Modulate Non-small Cell Lung Cancer Plasticity and Therapeutic
950 Response. Cancer Cell *27*, 698-711. 10.1016/j.ccell.2015.04.001.
951 Lou, K., Steri, V., Ge, A.Y., Hwang, Y.C., Yogodzinski, C.H., Shkedi, A.R., Choi, A.L.M., Mitchell, D.C.,
952 Swaney, D.L., Hann, B., et al. (2019). KRAS(G12C) inhibition produces a driver-limited state revealing
953 collateral dependencies. Sci Signal *12*. 10.1126/scisignal.aaw9450.
954 Mazumder, S., Choudhary, G.S., Al-Harbi, S., and Almasan, A. (2012). Mcl-1 Phosphorylation defines ABT-
955 737 resistance that can be overcome by increased NOXA expression in leukemic B cells. Cancer Res *72*,
956 3069-3079. 10.1158/0008-5472.CAN-11-4106.

bioRxiv preprint doi: https://doi.org/10.1101/2022.09.29.510137; this version posted September 30, 2022. The copyright holder for this preprint (which was not certified by peer review) is the author/funder, who has granted bioRxiv a license to display the preprint in perpetuity. It is made available under aCC-BY-NC-ND 4.0 International license.

957 Misale, S., Fatherree, J.P., Cortez, E., Li, C., Bilton, S., Timonina, D., Myers, D.T., Lee, D., Gomez-
958 Caraballo, M., Greenberg, M., et al. (2019). KRAS G12C NSCLC Models Are Sensitive to Direct Targeting
959 of KRAS in Combination with PI3K Inhibition. Clin Cancer Res *25*, 796-807. 10.1158/1078-0432.CCR-18-
960 0368.
961 Montero, J., Sarosiek, K.A., DeAngelo, J.D., Maertens, O., Ryan, J., Ercan, D., Piao, H., Horowitz, N.S.,
962 Berkowitz, R.S., Matulonis, U., et al. (2015). Drug-induced death signaling strategy rapidly predicts
963 cancer response to chemotherapy. Cell *160*, 977-989. 10.1016/j.cell.2015.01.042.
964 Morel, C., Carlson, S.M., White, F.M., and Davis, R.J. (2009). Mcl-1 integrates the opposing actions of
965 signaling pathways that mediate survival and apoptosis. Mol Cell Biol *29*, 3845-3852.
966 10.1128/MCB.00279-09.
967 Murray, C.W., Brady, J.J., Han, M., Cai, H., Tsai, M.K., Pierce, S.E., Cheng, R., Demeter, J., Feldser, D.M.,
968 Jackson, P.K., et al. (2022). LKB1 drives stasis and C/EBP-mediated reprogramming to an alveolar type II
969 fate in lung cancer. Nat Commun *13*, 1090. 10.1038/s41467-022-28619-8.
970 Murray, C.W., Brady, J.J., Tsai, M.K., Li, C., Winters, I.P., Tang, R., Andrejka, L., Ma, R.K., Kunder, C.A.,
971 Chu, P., and Winslow, M.M. (2019). An LKB1-SIK Axis Suppresses Lung Tumor Growth and Controls
972 Differentiation. Cancer Discov *9*, 1590-1605. 10.1158/2159-8290.CD-18-1237.
973 Nakada, D., Saunders, T.L., and Morrison, S.J. (2010). Lkb1 regulates cell cycle and energy metabolism in
974 haematopoietic stem cells. Nature *468*, 653-658. 10.1038/nature09571.
975 Nangia, V., Siddiqui, F.M., Caenepeel, S., Timonina, D., Bilton, S.J., Phan, N., Gomez-Caraballo, M.,
976 Archibald, H.L., Li, C., Fraser, C., et al. (2018). Exploiting MCL1 Dependency with Combination MEK +
977 MCL1 Inhibitors Leads to Induction of Apoptosis and Tumor Regression in KRAS-Mutant Non-Small Cell
978 Lung Cancer. Cancer Discov. 10.1158/2159-8290.CD-18-0277.
979 Ni Chonghaile, T., Sarosiek, K.A., Vo, T.T., Ryan, J.A., Tammareddi, A., Moore Vdel, G., Deng, J., Anderson,
980 K.C., Richardson, P., Tai, Y.T., et al. (2011). Pretreatment mitochondrial priming correlates with clinical
981 response to cytotoxic chemotherapy. Science *334*, 1129-1133. 10.1126/science.1206727.
982 Pan, R., Ruvolo, V., Mu, H., Leverson, J.D., Nichols, G., Reed, J.C., Konopleva, M., and Andreeff, M.
983 (2017). Synthetic Lethality of Combined Bcl-2 Inhibition and p53 Activation in AML: Mechanisms and
984 Superior Antileukemic Efficacy. Cancer Cell *32*, 748-760 e746. 10.1016/j.ccell.2017.11.003.
985 Park, G.B., Choi, Y., Kim, Y.S., Lee, H.K., Kim, D., and Hur, D.Y. (2014). ROS-mediated JNK/p38-MAPK
986 activation regulates Bax translocation in Sorafenib-induced apoptosis of EBV-transformed B cells. Int J
987 Oncol *44*, 977-985. 10.3892/ijo.2014.2252.
988 Pierce, S.E., Granja, J.M., Corces, M.R., Brady, J.J., Tsai, M.K., Pierce, A.B., Tang, R., Chu, P., Feldser, D.M.,
989 Chang, H.Y., et al. (2021). LKB1 inactivation modulates chromatin accessibility to drive metastatic
990 progression. Nat Cell Biol *23*, 915-924. 10.1038/s41556-021-00728-4.
991 Pooya, S., Liu, X., Kumar, V.B., Anderson, J., Imai, F., Zhang, W., Ciraolo, G., Ratner, N., Setchell, K.D.,
992 Yoshida, Y., et al. (2014). The tumour suppressor LKB1 regulates myelination through mitochondrial
993 metabolism. Nat Commun *5*, 4993. 10.1038/ncomms5993.
994 Pumiglia, K.M., and Decker, S.J. (1997). Cell cycle arrest mediated by the MEK/mitogen-activated protein
995 kinase pathway. Proc Natl Acad Sci U S A *94*, 448-452. 10.1073/pnas.94.2.448.
996 Ricciuti, B., Arbour, K.C., Lin, J.J., Vajdi, A., Vokes, N., Hong, L., Zhang, J., Tolstorukov, M.Y., Li, Y.Y., Spurr,
997 L.F., et al. (2022). Diminished Efficacy of Programmed Death-(Ligand)1 Inhibition in STK11- and KEAP1-
998 Mutant Lung Adenocarcinoma Is Affected by KRAS Mutation Status. J Thorac Oncol *17*, 399-410.
999 10.1016/j.jtho.2021.10.013.
1000 Robitaille, K., Daviau, A., Lachance, G., Couture, J.P., and Blouin, R. (2008). Calphostin C-induced
1001 apoptosis is mediated by a tissue transglutaminase-dependent mechanism involving the DLK/JNK
1002 signaling pathway. Cell Death Differ *15*, 1522-1531. 10.1038/cdd.2008.77.

bioRxiv preprint doi: https://doi.org/10.1101/2022.09.29.510137; this version posted September 30, 2022. The copyright holder for this preprint (which was not certified by peer review) is the author/funder, who has granted bioRxiv a license to display the preprint in perpetuity. It is made available under aCC-BY-NC-ND 4.0 International license.

Rosellini, P., Amintas, S., Caumont, C., Veillon, R., Galland-Girodet, S., Cuguilliere, A., Nguyen, L., Domblides, C., Gouverneur, A., Merlio, J.P., et al. (2022). Clinical impact of STK11 mutation in advanced-stage non-small cell lung cancer. Eur J Cancer *172*, 85-95. 10.1016/j.ejca.2022.05.026.

Ryan, M.B., Fece de la Cruz, F., Phat, S., Myers, D.T., Wong, E., Shahzade, H.A., Hong, C.B., and Corcoran, R.B. (2020). Vertical Pathway Inhibition Overcomes Adaptive Feedback Resistance to KRAS(G12C) Inhibition. Clin Cancer Res *26*, 1633-1643. 10.1158/1078-0432.CCR-19-3523.

Shackelford, D.B., Abt, E., Gerken, L., Vasquez, D.S., Seki, A., Leblanc, M., Wei, L., Fishbein, M.C., Czernin, J., Mischel, P.S., and Shaw, R.J. (2013). LKB1 inactivation dictates therapeutic response of non-small cell lung cancer to the metabolism drug phenformin. Cancer Cell *23*, 143-158. 10.1016/j.ccr.2012.12.008.

Shackelford, D.B., and Shaw, R.J. (2009). The LKB1-AMPK pathway: metabolism and growth control in tumour suppression. Nat Rev Cancer *9*, 563-575. 10.1038/nrc2676.

Shaw, R.J., Bardeesy, N., Manning, B.D., Lopez, L., Kosmatka, M., DePinho, R.A., and Cantley, L.C. (2004a). The LKB1 tumor suppressor negatively regulates mTOR signaling. Cancer Cell *6*, 91-99. 10.1016/j.ccr.2004.06.007.

Shaw, R.J., Kosmatka, M., Bardeesy, N., Hurley, R.L., Witters, L.A., DePinho, R.A., and Cantley, L.C. (2004b). The tumor suppressor LKB1 kinase directly activates AMP-activated kinase and regulates apoptosis in response to energy stress. Proc Natl Acad Sci U S A *101*, 3329-3335. 10.1073/pnas.0308061100.

Shelly, M., Cancedda, L., Heilshorn, S., Sumbre, G., and Poo, M.M. (2007). LKB1/STRAD promotes axon initiation during neuronal polarization. Cell *129*, 565-577. 10.1016/j.cell.2007.04.012.

Singh, A., Greninger, P., Rhodes, D., Koopman, L., Violette, S., Bardeesy, N., and Settleman, J. (2009). A gene expression signature associated with "K-Ras addiction" reveals regulators of EMT and tumor cell survival. Cancer Cell *15*, 489-500. 10.1016/j.ccr.2009.03.022.

Skoulidis, F., Byers, L.A., Diao, L., Papadimitrakopoulou, V.A., Tong, P., Izzo, J., Behrens, C., Kadara, H., Parra, E.R., Canales, J.R., et al. (2015). Co-occurring genomic alterations define major subsets of KRAS-mutant lung adenocarcinoma with distinct biology, immune profiles, and therapeutic vulnerabilities. Cancer Discov *5*, 860-877. 10.1158/2159-8290.CD-14-1236.

Skoulidis, F., Goldberg, M.E., Greenawalt, D.M., Hellmann, M.D., Awad, M.M., Gainor, J.F., Schrock, A.B., Hartmaier, R.J., Trabucco, S.E., Gay, L., et al. (2018). STK11/LKB1 Mutations and PD-1 Inhibitor Resistance in KRAS-Mutant Lung Adenocarcinoma. Cancer Discov. 10.1158/2159-8290.CD-18-0099.

Skoulidis, F., Li, B.T., Dy, G.K., Price, T.J., Falchook, G.S., Wolf, J., Italiano, A., Schuler, M., Borghaei, H., Barlesi, F., et al. (2021). Sotorasib for Lung Cancers with KRAS p.G12C Mutation. N Engl J Med *384*, 2371-2381. 10.1056/NEJMoa2103695.

Tong, J., Zheng, X., Tan, X., Fletcher, R., Nikolovska-Coleska, Z., Yu, J., and Zhang, L. (2018). Mcl-1 Phosphorylation without Degradation Mediates Sensitivity to HDAC Inhibitors by Liberating BH3-Only Proteins. Cancer Res *78*, 4704-4715. 10.1158/0008-5472.CAN-18-0399.

Tsuruta, F., Sunayama, J., Mori, Y., Hattori, S., Shimizu, S., Tsujimoto, Y., Yoshioka, K., Masuyama, N., and Gotoh, Y. (2004). JNK promotes Bax translocation to mitochondria through phosphorylation of 14-3-3 proteins. EMBO J *23*, 1889-1899. 10.1038/sj.emboj.7600194.

Van Nostrand, J.L., Hellberg, K., Luo, E.C., Van Nostrand, E.L., Dayn, A., Yu, J., Shokhirev, M.N., Dayn, Y., Yeo, G.W., and Shaw, R.J. (2020). AMPK regulation of Raptor and TSC2 mediate metformin effects on transcriptional control of anabolism and inflammation. Genes Dev *34*, 1330-1344. 10.1101/gad.339895.120.

Wagner, E.F., and Nebreda, A.R. (2009). Signal integration by JNK and p38 MAPK pathways in cancer development. Nat Rev Cancer *9*, 537-549. 10.1038/nrc2694.

Wingo, S.N., Gallardo, T.D., Akbay, E.A., Liang, M.C., Contreras, C.M., Boren, T., Shimamura, T., Miller, D.S., Sharpless, N.E., Bardeesy, N., et al. (2009). Somatic LKB1 mutations promote cervical cancer progression. PLoS One *4*, e5137. 10.1371/journal.pone.0005137.

bioRxiv preprint doi: https://doi.org/10.1101/2022.09.29.510137; this version posted September 30, 2022. The copyright holder for this preprint (which was not certified by peer review) is the author/funder, who has granted bioRxiv a license to display the preprint in perpetuity. It is made available under aCC-BY-NC-ND 4.0 International license.

Xue, J.Y., Zhao, Y., Aronowitz, J., Mai, T.T., Vides, A., Qeriqi, B., Kim, D., Li, C., de Stanchina, E., Mazutis, L., et al. (2020). Rapid non-uniform adaptation to conformation-specific KRAS(G12C) inhibition. Nature *577*, 421-425. 10.1038/s41586-019-1884-x.

Yuan, D., Huang, S., Berger, E., Liu, L., Gross, N., Heinzmann, F., Ringelhan, M., Connor, T.O., Stadler, M., Meister, M., et al. (2017). Kupffer Cell-Derived Tnf Triggers Cholangiocellular Tumorigenesis through JNK due to Chronic Mitochondrial Dysfunction and ROS. Cancer Cell *31*, 771-789 e776. 10.1016/j.ccell.2017.05.006.

Zagorska, A., Deak, M., Campbell, D.G., Banerjee, S., Hirano, M., Aizawa, S., Prescott, A.R., and Alessi, D.R. (2010). New roles for the LKB1-NUAK pathway in controlling myosin phosphatase complexes and cell adhesion. Sci Signal *3*, ra25. 10.1126/scisignal.2000616.

Zhang, H., Fillmore Brainson, C., Koyama, S., Redig, A.J., Chen, T., Li, S., Gupta, M., Garcia-de-Alba, C., Paschini, M., Herter-Sprie, G.S., et al. (2017). Lkb1 inactivation drives lung cancer lineage switching governed by Polycomb Repressive Complex 2. Nat Commun *8*, 14922. 10.1038/ncomms14922.

bioRxiv preprint doi: https://doi.org/10.1101/2022.09.29.510137; this version posted September 30, 2022. The copyright holder for this preprint (which was not certified by peer review) is the author/funder, who has granted bioRxiv a license to display the preprint in perpetuity. It is made available under aCC-BY-NC-ND 4.0 International license.

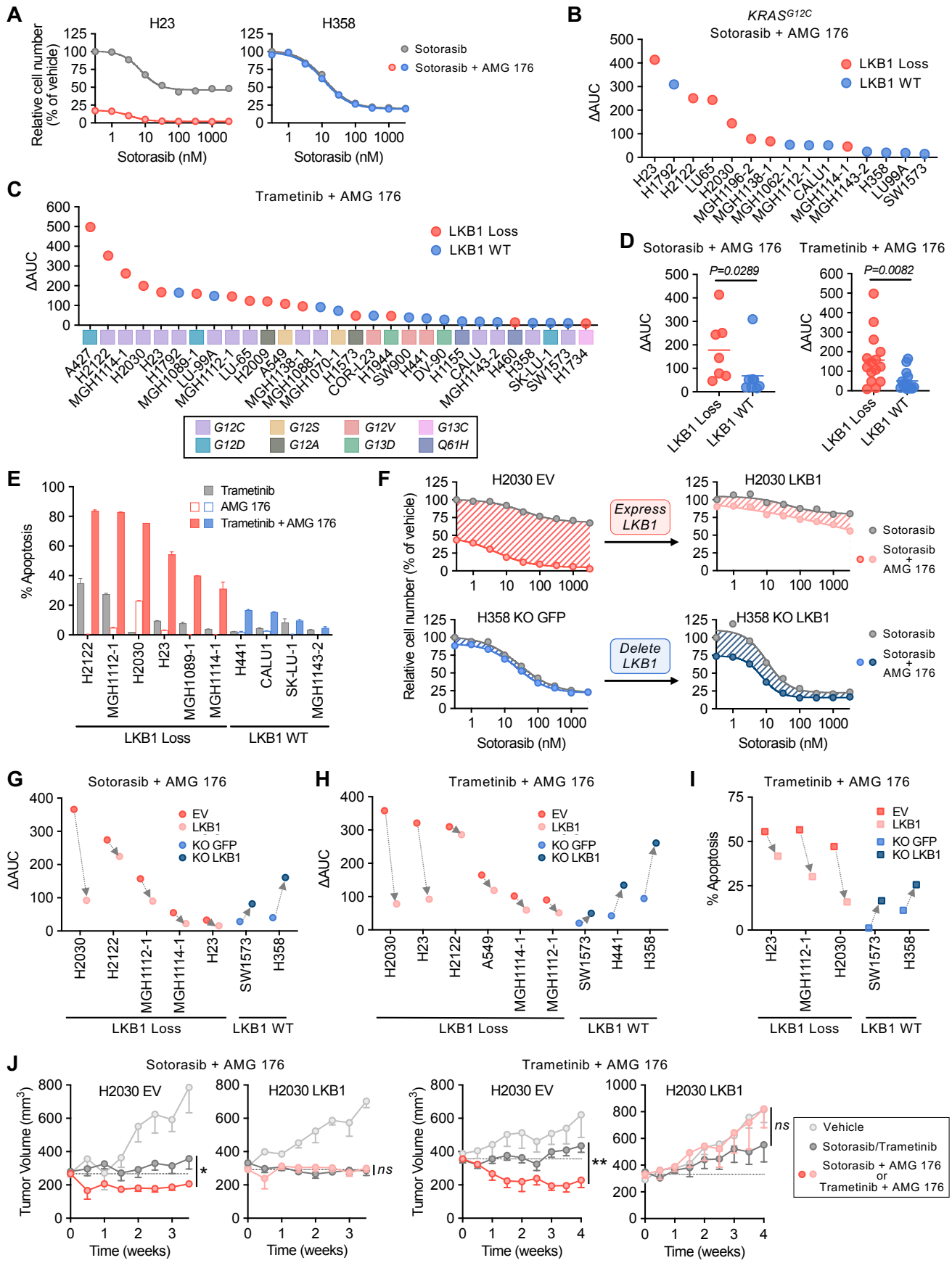

Figure 1. LKB1 loss confers sensitivity to combined MAPK + MCL-1 inhibition in *KRAS*-mutant NSCLC models

bioRxiv preprint doi: https://doi.org/10.1101/2022.09.29.510137; this version posted September 30, 2022. The copyright holder for this preprint (which was not certified by peer review) is the author/funder, who has granted bioRxiv a license to display the preprint in perpetuity. It is made available under aCC-BY-NC-ND 4.0 International license.

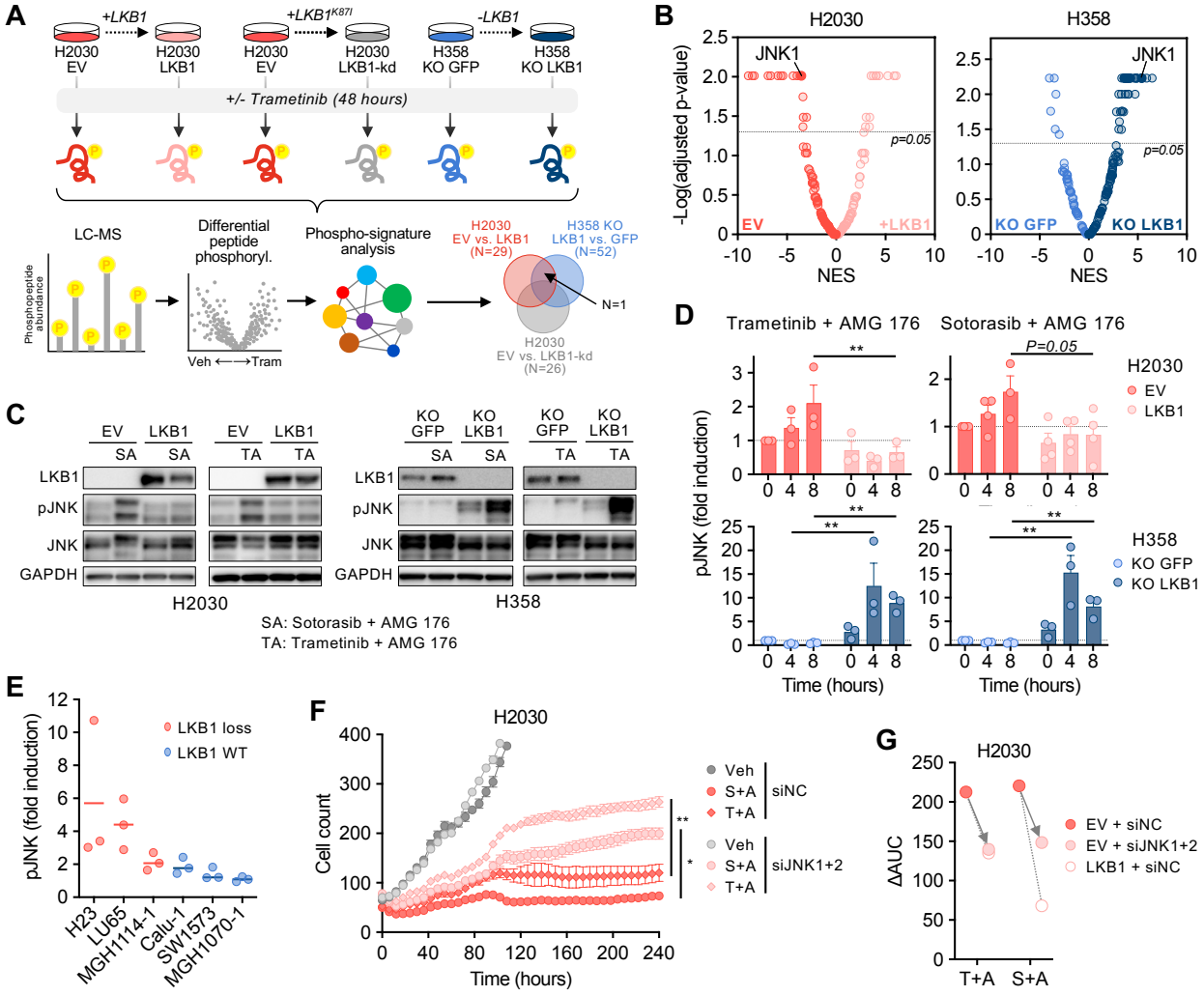

Figure 2. JNK activation in LKB1-deficient cells underlies sensitivity to MCL-1 inhibition

bioRxiv preprint doi: https://doi.org/10.1101/2022.09.29.510137; this version posted September 30, 2022. The copyright holder for this preprint (which was not certified by peer review) is the author/funder, who has granted bioRxiv a license to display the preprint in perpetuity. It is made available under aCC-BY-NC-ND 4.0 International license.

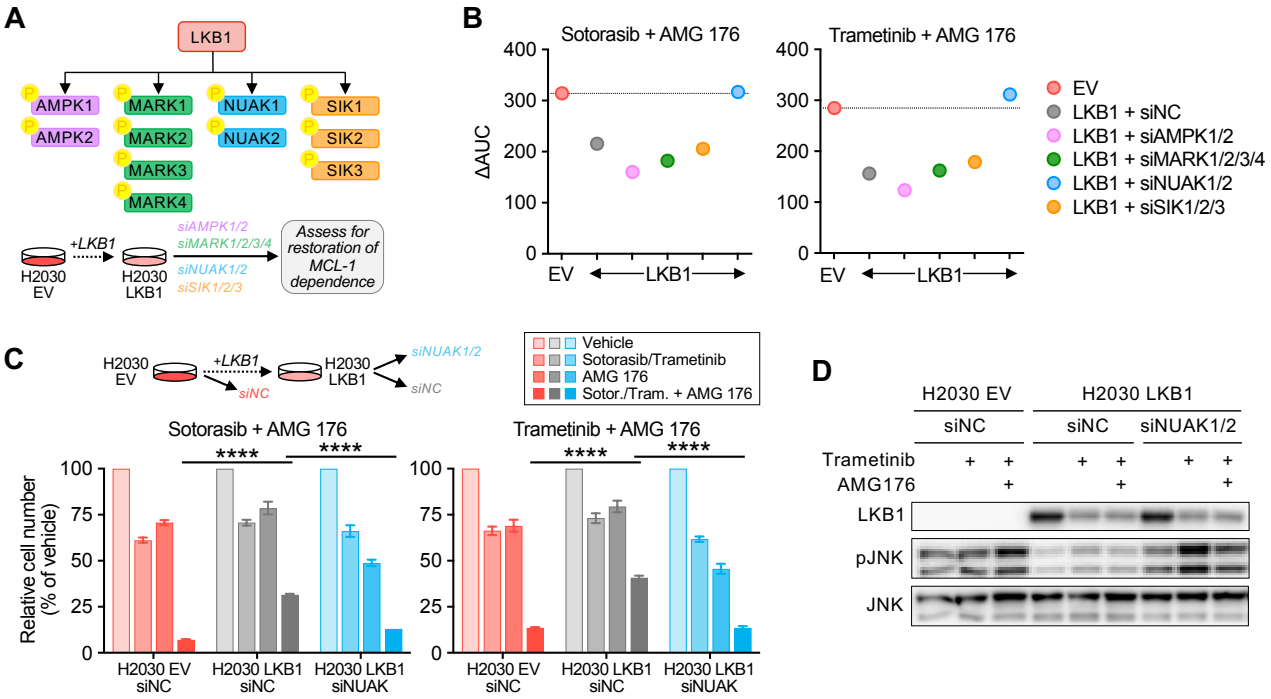

Figure 3. Suppression of JNK activation by LKB1 is mediated by NUAK kinases

bioRxiv preprint doi: https://doi.org/10.1101/2022.09.29.510137; this version posted September 30, 2022. The copyright holder for this preprint (which was not certified by peer review) is the author/funder, who has granted bioRxiv a license to display the preprint in perpetuity. It is made available under aCC-BY-NC-ND 4.0 International license.

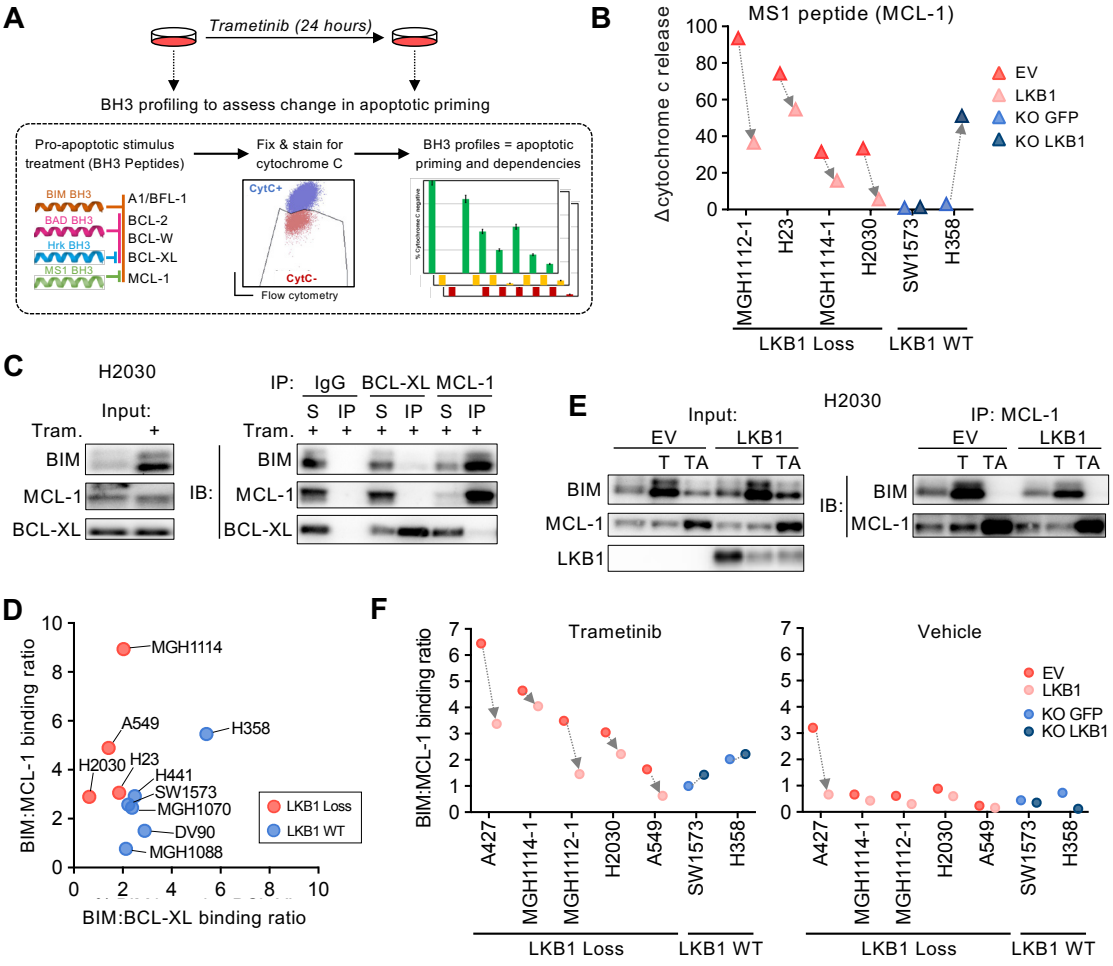

Figure 4. LKB1 loss increases BIM:MCL-1 interaction and creates an MCL-1 dependent state.

bioRxiv preprint doi: https://doi.org/10.1101/2022.09.29.510137; this version posted September 30, 2022. The copyright holder for this preprint (which was not certified by peer review) is the author/funder, who has granted bioRxiv a license to display the preprint in perpetuity. It is made available under aCC-BY-NC-ND 4.0 International license.

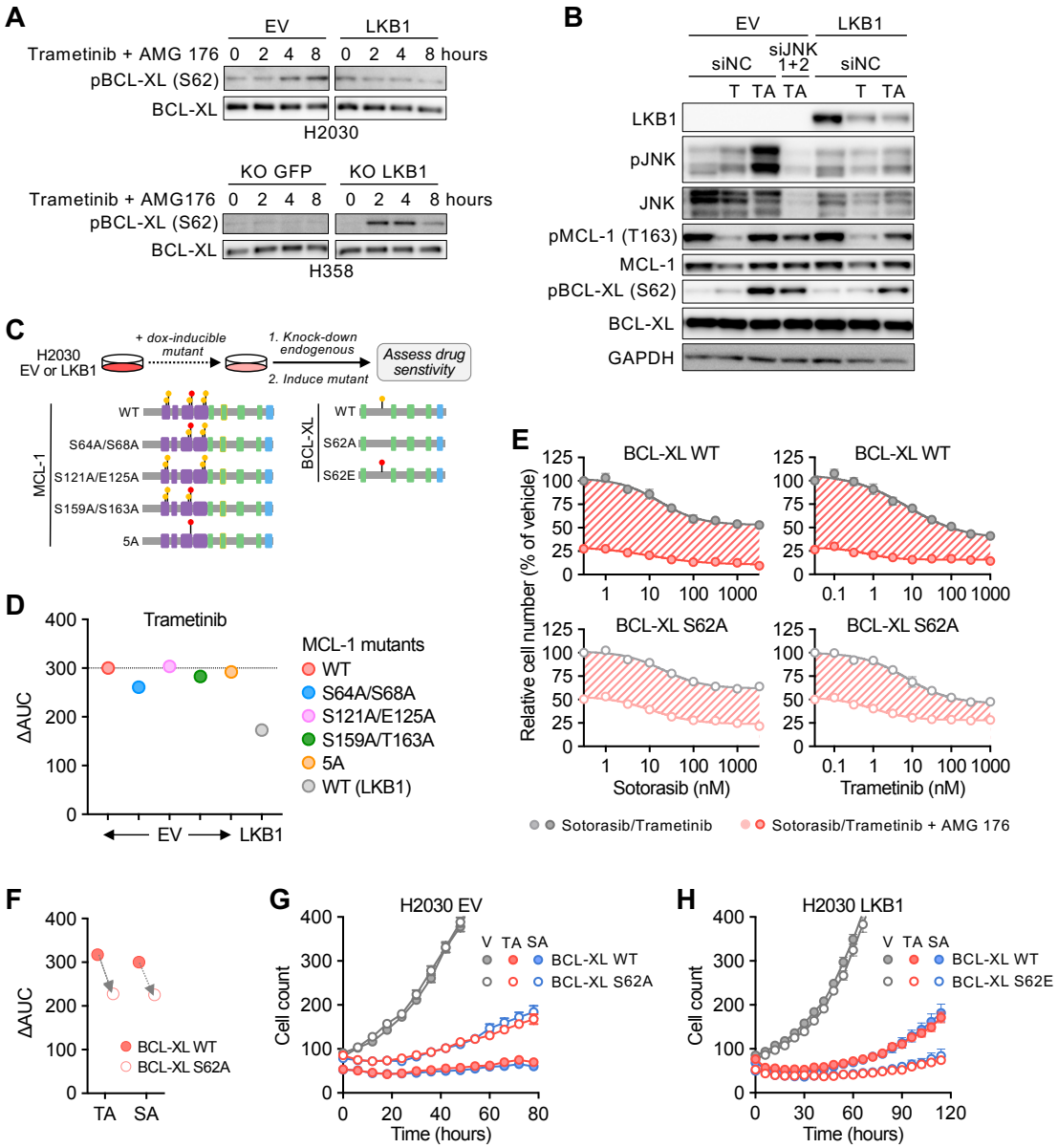

Figure 5. JNK phosphorylates BCL-XL to drive an MCL-1 dependent state

bioRxiv preprint doi: https://doi.org/10.1101/2022.09.29.510137; this version posted September 30, 2022. The copyright holder for this preprint (which was not certified by peer review) is the author/funder, who has granted bioRxiv a license to display the preprint in perpetuity. It is made available under aCC-BY-NC-ND 4.0 International license.

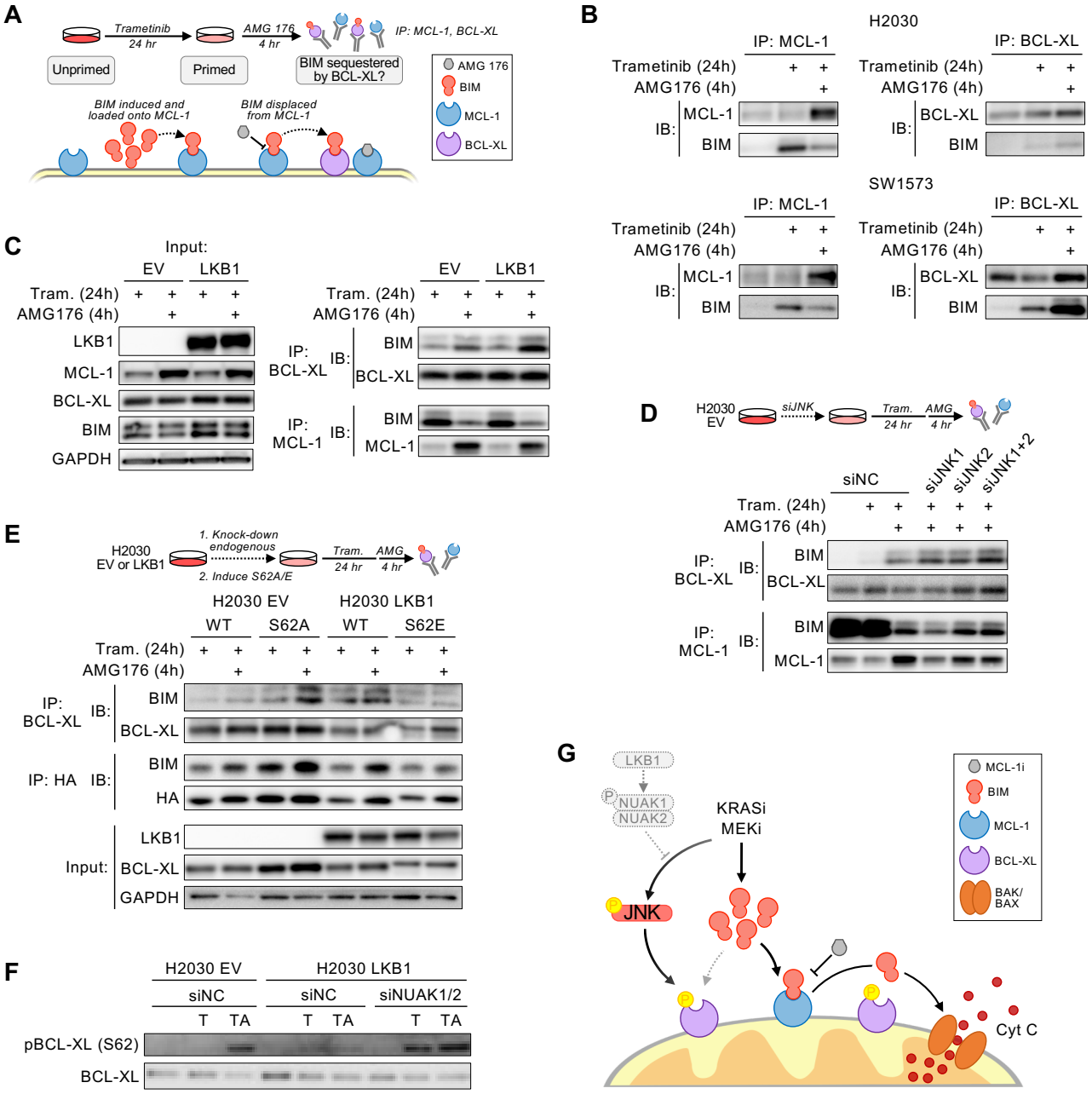

Figure 6. JNK activation drives an MCL-1 dependent state by modulating BIM:BCL-XL interactions.

bioRxiv preprint doi: https://doi.org/10.1101/2022.09.29.510137; this version posted September 30, 2022. The copyright holder for this preprint (which was not certified by peer review) is the author/funder, who has granted bioRxiv a license to display the preprint in perpetuity. It is made available under aCC-BY-NC-ND 4.0 International license.

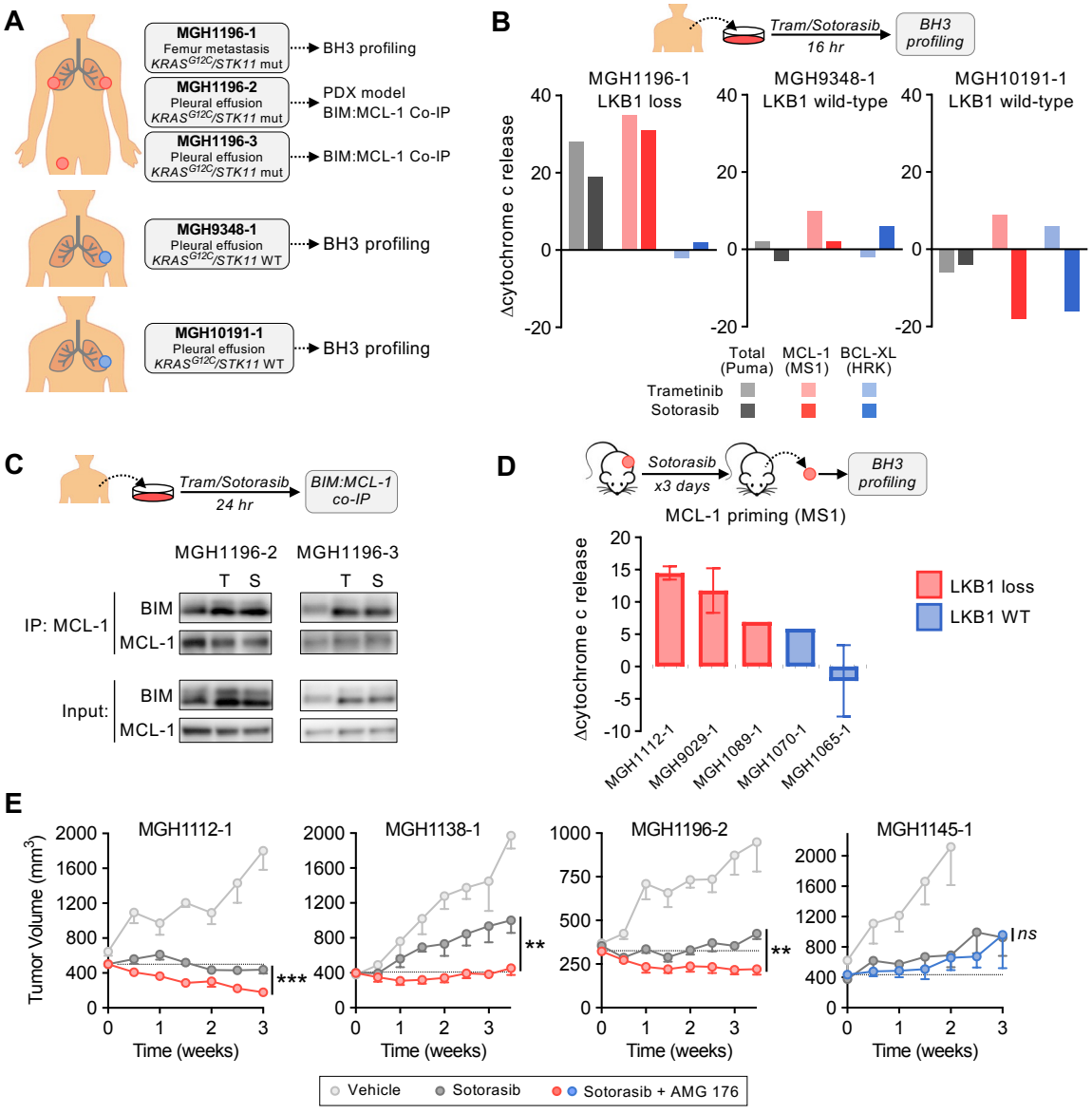

Figure 7. LKB1 loss predicts sensitivity to KRAS^{G12C} + MCL-1 inhibition in *KRAS^{G12C}*-mutant NSCLC PDX tumors and patient tumor explants.